The lipid phosphatase-like protein PLPPR1 increases cell adhesion by modulating RhoA/Rac1 activity

Chinyere Agbaegbu Iweka[1,2#], Sharada Tilve[1#], Yasuhiro Katagiri[1], Herbert M Geller[1*]

[1]Laboratory of Developmental Neurobiology, National Heart Lung and Blood Institute, NIH, Bethesda, MD.

[2]Department of Neuroscience, Interdisciplinary Program in Neuroscience, Georgetown University, Washington, DC.

[#] These authors contributed equally to this work.

***Correspondence:**

Herbert M. Geller (E-mail: gellerh@nhlbi.nih.gov)

Laboratory of Developmental Neurobiology

Cell Biology and Physiology Center

National Heart, Lung, and Blood Institute

National Institutes of Health

9000 Rockville Pike

Bethesda, MD 20892

Phone: 301-451-9440

FAX: 301-594-8133

Running Title: PLPPR1 increases cell adhesion

SUMMARY

PLPPR1 alters cytoskeletal dynamics to influence cell adhesion by modulating RhoA and Rac1 activation through its association with RhoGDI, enabling PLPPR1 to impede the inhibitory activity of CSPGs and LPA.

ABSTRACT

Phospholipid Phosphatase-Related Protein Type 1 (PLPPR1) is a member of a family of lipid phosphatase related proteins, integral membrane proteins characterized by six transmembrane domains. This family of proteins is enriched in the brain and recent data indicate potential pleiotropic functions in several different contexts. An inherent ability of this family of proteins is to induce membrane protrusions, and we have previously reported that members of this family may act in concert. However, the function of PLPPR1 is not yet understood. Here, we report that exogenous expression of PLPPR1 increases cell adhesion to the ECM substrate by altering cytoskeletal dynamics and modulating RhoA and Rac1 activity through association with RhoGDI, enabling PLPPR1 to overcome the inhibitory activity of CSPGs and LPA. Together, these results establish a novel signaling pathway for PLPPR1 protein.

44 **Abbreviations:** PLPPR (Phospholipid Phosphatase-Related Protein), PRG (Plasticity-Related
45 Gene), FA (Focal Adhesions), CSPG (Chondroitin Sulfate Proteoglycan), PLL (Poly-L-Lysine),
46 LPA (Lysosphosphatidic Acid), LPP (Lipid Phosphate Phosphatase), FAFBSA (Fatty Acid Free
47 Bovine Serum Albumin), MLC (myosin light chain II), MYPT1 (myosin light chain phosphatase
48 1), ERM (Ezrin, Radixin and Moesin), GSK (Glycogen Synthase Kinase), GEF (Guanine
49 Exchange Factor), GAP (GTPase Activating Protein), RhoGDI (Rho Guanine Nucleotide
50 Dissociation Inhibitor), IRM (Interference Reflection Microscopy), TIRF (Total Internal Reflection
51 Fluorescence), STED (Stimulated Emission Depletion).
52
53
54

55 **INTRODUCTION**

56 The Phospholipid Phosphatase Related (PLPPR) proteins (PLPPR1 – PLPPR5) are
57 highly enriched in the brain and their expression is regulated, with the highest expression levels
58 during development (Wang and Molnár, 2005). This family of proteins were originally named
59 "Plasticity-Related Genes", due to the upregulation of PLPPR4, the first protein of this family to
60 be discovered, in sprouting axons following hippocampal deafferentation (Brauer et al., 2003).
61 More recent studies have shown that expression of PLPPR1 mRNA correlates with sprouting
62 corticospinal axons after injury (Fink et al., 2017) and neuronal remodeling in the hippocampus
63 after kainaic acid treatment (Savaskan et al., 2004). Furthermore, decreased PLPPR1 mRNA
64 has been associated with dysregulated neuronal migration (Khalaf-Nazzal et al., 2017; Pfurr et
65 al., 2017), suggesting a role for these proteins in neuronal migration as well as neurogenesis
66 and axon growth after injury.

67 We and others have previously shown that overexpression of PLPPR1 induces actin-rich
68 membrane protrusions in many different cell types (Broggini et al., 2016; Sigal et al., 2007;
69 Velmans et al., 2013; Yu et al., 2015). Overexpression of PLPPR5, the closest relative of
70 PLPPR1 in this family, produces a similar phenotype (Broggini et al., 2010). The members of
71 this family interact with each other and may function as a heteromeric complex in causing these
72 phenotypic changes (Yu et al., 2015), suggesting that these proteins may alter cytoskeletal
73 dynamics to induce membrane protrusions. However, the mechanism by which the PLPPR1
74 protein mediates this morphological change is yet unknown.

75 Here, we report that PLPPR1 overexpression leads to increased cell adhesion due to
76 changes in cytoskeletal dynamics. This increased adhesion results in decreased cell migration
77 as well as the ability of cells overexpressing PLPPR1 to overcome the inhibitory activity of
78 lysophosphatidic acid (LPA) and chondroitin sulfate proteoglycans (CSPGs). These changes in
79 cell adhesion are due to alterations in the RhoA-ROCK signaling pathway mediated by PLPPR1

80 through association with RhoGDI. Together, these results establish a novel signaling pathway
81 for the PLPPR family of proteins.
82
83 **RESULTS**
84 **PLPPR1 reduces cell migration and increases cell adhesion**
85 Overexpression of PLPPR1 induces actin-rich membrane protrusions in several different
86 cell types (Broggini et al., 2016; Savaskan et al., 2004; Sigal et al., 2007; Velmans et al., 2013;
87 Yu et al., 2015) implying a change in cytoskeletal dynamics. Many cellular processes including
88 cell migration and cell adhesion require dynamic changes to the cytoskeleton. Therefore, using
89 live cell imaging, we traced the migratory trajectories of individual Neuro2a cells expressing
90 either EGFP or EGFP-PLPPR1 on a uniform fibronectin substrate at a concentration determined
91 to be permissive for cell migration (Fig. 1A). We found that the average speed (Fig. 1B) and
92 average distance travelled by migrating cells overexpressing PLPPR1 (Fig. 1C) was significantly
93 reduced compared to EGFP-transfected cells.
94 Cell adhesion is a major determinant for cell migration and tissue morphogenesis. To
95 determine if PLPPR1 had any effect on cell adhesion, we performed a time-dependent cell
96 adhesion assay on Neuro2a cells expressing either EGFP or EGFP-PLPPR1. Our results show
97 that overexpression of PLPPR1 increased cell adhesion on a fibronectin substrate (Fig. 2A, B,
98 Fig. S1).
99 The PLPPR family share high sequence homology with the exception of their C-terminal
100 domain. Additionally, since the C-terminus of PLPPR1 is unique and essential to its ability to
101 induce membrane protrusions (Broggini et al., 2016; Yu et al., 2015), we questioned if the C-
102 terminal domain is essential to its ability to resist detachment from the fibronectin substrate.
103 Therefore, we deleted the 43 amino acid residues constituting the C-terminus of PLPPR1 and
104 expressed EGFP-PLPPR1ΔC43 in Neuro2a cells. We found that EGFP-PLPPR1ΔC43 also

105 resisted detachment to the fibronectin substrate after extensive washing, indicating that the
106 ability of PLPPR1 to increase cell adhesion is independent of its C-terminal domain (Fig. 2A, B).
107 Next, to examine the degree of attachment in cells overexpressing PLPPR1, we used
108 Interference Reflection Microscopy (IRM) imaging to observe and quantify events at the
109 interface between the cell surface and the fibronectin substrate. With IRM, the very fine cell
110 contours and the degree of contact cells exert on the fibronectin substrate can be visualized and
111 measured. Cell membranes in close contact with the substrate produce more interference and
112 darker pixels while membranes further from the substrate have less interference and hence,
113 lighter pixels (Fig. 2C). IRM imaging showed that the average area of attachment to the
114 fibronectin substrate was significantly greater in cells overexpressing PLPPR1 suggesting a
115 stronger adherence compared to EGFP-transfected cells (Fig. 2D). This confirms our results
116 that show increased resistance to detachment by trypsin/EDTA in cells overexpressing PLPPR1
117 (Fig. S1).
118 Our previous studies have demonstrated that while cytochalasin treatment eliminated
119 most of the membrane protrusions induced by overexpression of PLPPR1, some still remained,
120 suggesting that not all the protrusions induced by PLPPR1 contained actin filaments (Yu et al.,
121 2015). Using live-cell IRM imaging, we observed that some of these protrusions induced by
122 PLPPR1 remained strongly adhered to the ECM substrate, leaving a trail of fibrous structures as
123 the cell migrates (Video 1, Fig. 2E, F). To confirm that these trailing fibers are devoid of actin
124 filaments, we co-expressed mApple-FTR-940 (F-tractin) with either EGFP or EGFP-PLPPR1 in
125 Neuro2a cells. Confocal images show that these “trailing fibers” indeed lack actin filaments (Fig.
126 2G). The presence of such “trailing fibers”, devoid of cytoskeletal components, have been
127 attributed to active migration in cancer cells (DePasquale, 1998; Haemmerli and Strauli, 1981)
128 and a stronger adherence of the cells to their substrate. Together, these results show that
129 overexpression of PLPPR1 decreases cell migration due to increased adhesion to the
130 fibronectin substrate.

131 **PPLRI promotes the destabilization of actin cytoskeleton**

132 The dynamic organization of the actin cytoskeleton causes changes in cell shape and
133 adhesion strength. This generates sufficient tension to create the pushing and pulling forces that
134 enable cell migration (Gardel et al., 2010; van Helvert et al., 2018). Confocal imaging
135 demonstrated that cells overexpressing PLPPR1 lack the network of organized linear stress
136 fibers observed in the cell periphery of EGFP-transfected cells (Fig. 3A). Since actin
137 polymerization and depolymerization are required for cell migration (Mogilner and Oster, 1996;
138 Ridley et al., 2003), actin turnover was determined by FRAP measurements in cells co-
139 expressing F-tractin with either EGFP or EGFP-PLPPR1 (Fig. 3B). The leading edge of the cell
140 was photo-bleached and fluorescence recovery was recorded. Results show a decrease in the
141 rate of fluorescence recovery of F-tractin in cells overexpressing PLPPR1 (Fig. 3C) with a short
142 half-time compared to EGFP-transfected cells (Fig. 3D). The mobile fraction of monomeric actin
143 was also decreased in cells overexpressing PLPPR1 compared to EGFP-transfected cells (Fig.
144 3E). Together, these results show a decrease in the rate of actin polymerization, suggesting
145 destabilized actin in cells overexpressing PLPPR1.

146

147 **PLPPR1 increases nascent focal adhesions**

148 The increased cell adhesion observed in cells overexpressing PLPPR1 led us to
149 evaluate changes in focal adhesion (FA) dynamics. Paxillin is expressed at focal adhesion sites,
150 therefore, cells expressing either EGFP or EGFP-PLPPR1 were plated on a fibronectin
151 substrate and immunostained for paxillin and F-actin (Fig. 4A). TIRF imaging revealed that the
152 distinct ventral stress fibers in the well-defined lamellipodial structure observed in EGFP-
153 transfected cells were absent in cells overexpressing PLPPR1 (white asterisks, Fig. 4A).
154 Additionally, F-actin containing stress fibers were sparse in cells overexpressing PLPPR1
155 compared to EGFP-transfected cells (Fig. 4A).

156 Focal adhesions (FA) are mechanosensitive and require the recruitment of several
157 proteins in order to change their composition and mature (Pasapera et al., 2010). This tension-
158 mediated maturation involves the recruitment of paxillin to nascent focal adhesion complexes
159 that are initially small in size, but then mature into focal adhesions as the size of the focal
160 complexes increase and are stabilized (Pasapera et al., 2010; Zaidel-Bar et al., 2003).
161 Measurement of the size of individual FA revealed more nascent paxillin in cells overexpressing
162 PLPPR1, compared to EGFP-transfected cells, suggesting reduced FA turnover (Fig. 4B). Live
163 cell imaging confirmed that the focal adhesion complexes in cells co-expressing EGFP-PLPPR1
164 and mCherry-paxillin remained nascent compared to the mature FA observed in EGFP-
165 transfected cells (Video 2). Furthermore, the average fluorescence intensity of paxillin-positive
166 FA was significantly increased in cells overexpressing PLPPR1 compared to EGFP-transfected
167 cells (Fig. 4C).
168 Phosphorylation of paxillin on Y31 is crucial for regulation of paxillin turnover and focal
169 adhesion maturation (Zaidel-Bar et al., 2007). Immunoblotting of cell lysates from Neuro2a cells
170 expressing either EGFP or EGFP-PLPPR1 revealed an increase in phosphorylation of paxillin in
171 cells overexpressing PLPPR1 (Fig. 4D, E). Paxillin phosphorylation at Y31 is mediated by FAK
172 (Bellis et al., 1995; Schaller and Parsons, 1995), therefore, we evaluated phosphorylation levels
173 of FAK. Phosphorylation of FAK at Y576 in cells overexpressing PLPPR1 was increased
174 compared to EGFP-transfected cells (Fig. 4D, F). Altogether, these results demonstrate reduced
175 stability and size of focal adhesions, due to increased phosphorylation of paxillin and FAK in
176 cells overexpressing PLPPR1.
177
178 **PLPPR1 overcomes CSPG inhibition of neurite outgrowth.**
179 Overexpression of PLPPR1 protein can overcome the inhibitory activity of myelin as well
180 as LPA-induced axon collapse and neurite retraction (Broggini et al., 2016). Furthermore,
181 PLPPR1 has been demonstrated to promote axon regeneration after spinal cord injury in mice

182 (Fink et al., 2017). Chondroitin sulfate proteoglycans are universally upregulated in the glial scar
183 following injury and are potent negative regulators of axon growth (Davies et al., 1999; Hynds
184 and Snow, 1999; Schwab et al., 1993). Therefore, we asked if overexpression of PLPPR1 could
185 overcome the inhibitory activity of CSPGs. Hippocampal neurons were transfected with EGFP
186 or EGFP-PLPPR1 and seeded on glass coverslips coated with either poly-L-lysine (PLL) or PLL
187 and CSPGs. Neurite outgrowth was analyzed by measuring both total neurite length and longest
188 neurite (Fig. 5A). Total neurite length of EGFP and EGFP-PLPPR1 transfected neurons plated
189 on PLL alone were 86.1 ± 6.5μm and 90.4 ± 6.1μm respectively. However, in the presence of
190 CSPGs, total neurite length was markedly decreased in EGFP-transfected neurons, 53.8 ±
191 4.4μm, $p<0.001$, (Fig. 5B). In comparison, total neurite length of neurons overexpressing
192 PLPPR1 exposed to CSPGs was not significantly different from neurons plated on PLL alone,
193 94.8 ± 6.0μm. Similarly, we observed a decrease in the length of the longest neurite of EGFP-
194 transfected neurons, while this inhibition was not observed in neurons overexpressing PLPPR1
195 (Fig. 5C). These results demonstrate that overexpression of PLPPR1 impedes the inhibitory
196 activity of CSPGs on neurite outgrowth.

197 Modulation of axon growth by PLPPR1 has been reported to be dependent on its C-
198 terminal domain (Broggini et al., 2016). Therefore, we expressed EGFP-PLPPR1ΔC43 in
199 Neuro2a cells and assessed its ability to overcome CSPG inhibition of neurite outgrowth (Fig.
200 S2A). Our results show no difference in total neurite length or in the longest neurite between
201 neurons expressing EGFP or EGFP-PLPPR1 on PLL alone. However, neurons expressing
202 PLPPR1ΔC43 had shorter neurites (Fig. S2B). This difference suggests that overexpression of
203 PLPPR1ΔC43, by itself, may interfere with neurite outgrowth, probably due to improper protein
204 localization as most of the truncated PLPPR1 protein tends to be retained in the endoplasmic
205 reticulum (Yu et al., 2015). In contrast, while EGFP-transfected neurons exhibited significant
206 decrease in total neurite length and longest neurite when plated onto CSPGs, the total neurite

207 length and the longest neurite of neurons expressing full-length PLPPR1 and PLPPR1ΔC43
208 remained unchanged suggesting that the ability to overcome CSPG inhibition is not dependent
209 on the C-terminus of PLPPR1 (Fig. S2B, C).
210

211 **PLPPR1 attenuates LPA-induced neurite retraction.**

212 LPA induces neurite retraction and cell rounding in several different cell types (Jalink et
213 al., 1993; Kranenburg et al., 1999; Tigyi et al., 1996). To confirm this in Neuro2a cells, serum
214 starved cells were exposed to either fatty acid free bovine serum albumin (FAFBSA) or LPA.
215 Live cell imaging revealed significant neurite retraction and cell rounding in cells exposed to
216 LPA compared to FAFBSA (Fig. S3A, Video 3A, B). Next, the effects of PLPPR1
217 overexpression on neurite retraction induced by LPA was examined. Neuro2a cells transfected
218 with EGFP or EGFP-PLPPR1 were exposed to either FAFBSA or LPA. 59% of cells expressing
219 EGFP underwent cell rounding and neurite retraction in response to LPA compared to 42% of
220 cells expressing EGFP-PLPPR1, $p<0.05$, (Fig. 5D, E), demonstrating the ability of PLPPR1 to
221 attenuate LPA activity. Additionally, expression of PLPPR1ΔC43 resulted in a similar attenuated
222 response to LPA as full-length PLPPR1 (Fig. S3B, C), suggesting that the ability to impede LPA-
223 induced neurite retraction is not dependent on the C-terminus of PLPPR1.
224

225 **PLPPR1 modulates RhoA activation**

226 The RhoA signaling pathway is common to many molecules inhibitory to axon growth,
227 including CSPGs, myelin and LPA (Alabed et al., 2006; Jain et al., 2004; Kranenburg et al.,
228 1999; Monnier et al., 2003). Additionally, RhoA activation by LPA was reduced in cells
229 overexpressing PLPPR5, the closest relative to PLPPR1 (Broggini et al., 2010). Therefore, we
230 asked if PLPPR1 could similarly affect RhoA activation by LPA. Serum starved Neuro2a cells
231 expressing EGFP or EGFP-PLPPR1 were exposed to either FAFBSA, serum or LPA. Active
232 RhoA bound to GTP was immunoprecipitated using rhotekin-RBD beads and then subjected to

233 immunoblot analysis. While cells expressing EGFP had increased RhoA activation in response
234 to either serum or LPA, there was no change in RhoA activation in cells overexpressing
235 PLPPR1 (Fig. 5F, G).
236
237 **PLPPR1 decreases LPA-induced phosphorylation of ROCK targets.**
238 Rho-associated kinase (Rho-kinase/ROCK/ROK) is a major RhoA effector and is
239 implicated in the regulation of actinomyosin dynamics and inhibition of neurite outgrowth
240 (Amano et al., 1997; Lingor et al., 2007; Monnier et al., 2003). ROCK mediates its effect by
241 phosphorylating several substrates including cytoskeletal proteins, MLC, MYPT1 and the ERM
242 proteins (Kaneko-Kawano et al., 2012; Matsui et al., 1998; Riddick et al., 2008; Sutherland et
243 al., 2016; Yoneda et al., 2005). We evaluated the modulatory effect of PLPPR1 on the RhoA-
244 ROCK pathway by assessing the phosphorylation levels of several ROCK substrates in
245 response to LPA treatment. First, we measured the phosphorylation levels of MLC. Serum
246 starved Neuro2a cells expressing EGFP or EGFP-PLPPR1, were exposed to either FAFBSA,
247 serum or LPA and immunostained for phosphorylated MLC. Confocal imaging showed basal
248 levels of phosphorylated MLC with a diffuse cytoplasmic distribution after FAFBSA treatment
249 (Fig. 6A – C). However, in response to LPA, phosphorylation of MLC was increased and
250 localized to the plasma membrane in EGFP-transfected cells while no change in
251 phosphorylation levels of MLC was observed and the diffuse cytosolic localization was retained
252 in cells overexpressing PLPPR1 (Fig. 6A – C). GFP immunoblot of cell lysates from Neuro2a
253 cells expressing EGFP or EGFP-PLPPR1 and treated with either FAFBSA, serum or LPA show
254 that expression levels for both EGFP and EGFP-PLPPR1 does not change between treatment
255 conditions, FAFBSA, serum or LPA (Fig. 6D). Immunoblot analysis confirms the increase in
256 phosphorylation of MLC at S19 in EGFP-transfected cells, with no change in the phosphorylated
257 levels of MLC in cells overexpressing PLPPR1 (Fig. 6E, F). Similarly, phosphorylation of MYPT1

258 at T853 was increased in response to LPA treatment in EGFP-transfected cells while MYPT1
259 phosphorylation levels remained unchanged in cells overexpressing PLPPR1 (Fig. 6G, H).
260 Next, we evaluated the effect of PLPPR1 on LPA stimulated phosphorylation of the ERM
261 proteins. EGFP-transfected cells exhibited an increase in ERM phosphorylation in response to
262 LPA while phosphorylation levels of the ERM proteins in cells overexpressing PLPPR1
263 remained unchanged (Fig. 6I, J).
264 Activation of the ERM proteins results in their translocation to the plasma membrane
265 (Kim et al., 2011; Shaw et al., 1998). Therefore, we immunostained for phosphorylated ERM
266 proteins in cells expressing either EGFP or EGFP-PLPPR1. After FAFBSA treatment, cells
267 displayed low levels of phosphorylated ERM with a diffuse cytoplasmic distribution (Fig. S4).
268 However, exposure to LPA induced the translocation of phosphorylated ERM to the plasma
269 membrane in cells expressing EGFP while ERM localization remained unchanged in cells
270 overexpressing PLPPR1 (Fig. S4). Together, these results demonstrate that overexpression of
271 PLPPR1 attenuates phosphorylation of MLC, MYPT1 and the ERM proteins after LPA
272 stimulation.
273 Since LPA is known to induce phosphorylation of Akt, GSK3ß and Tau through
274 activation of the PI3K-PKB/Akt and PLCγ-PKC pathways respectively (Baudhuin et al., 2002;
275 Fang et al., 2002; Sayas et al., 2006), we asked if the effects of PLPPR1 overexpression extend
276 to these pathways. Immunoblot analysis of phosphorylation levels of GSK3ß at Y216 and S9, of
277 Tau at S396 and of Akt at S473 in transfected Neuro2a cells after LPA treatment, showed no
278 significant change in cells overexpressing PLPPR1 compared to EGFP-transfected cells (Fig.
279 S5).
280 To determine if overexpression of PLPPR1 had any effect on the phosphorylation levels
281 of MLC, ERM, MYPT1, Akt, GSK3ß or Tau without LPA stimulation, we performed an
282 immunoblot analysis of cell lysates from Neuro2a cells transfected with either EGFP or EGFP-
283 PLPPR1. Results show no significant changes in phosphorylation levels of these ROCK target

284 proteins in cells overexpressing PLPPR1 compared to EGFP-transfected cells (Fig. S6).
285 Altogether, these results demonstrate that PLPPR1 specifically attenuates activation of the
286 RhoA-ROCK signaling pathway in response to stimulation.
287

288 **PLPPR1 modulates RhoA and Rac1 activation via RhoGDI interaction**

289 Previously, we identified RhoGDI as a possible binding partner for PLPPR1 (Yu et al.,
290 2013). By direct interaction with the Rho GTPases, RhoGDI prevents their translocation from
291 the cytosol to the plasma membrane thereby preventing the nucleotide exchange of GDP for
292 GTP (Boulter et al., 2010; Dovas and Couchman, 2005; Sabbatini and Williams, 2013). To
293 confirm the interaction between RhoGDI and PLPPR1, we immunoprecipitated EGFP-PLPPR1
294 using GFP magnetic/agarose beads and immunoblotted for RhoGDI. We also
295 immunoprecipitated EGFP-PLPPR1ΔC43, to determine if this putative interaction is dependent
296 on the C-terminal domain. Our results show that both EGFP-PLPPR1 and EGFP-PLPPR1ΔC43
297 co-immunoprecipitated with RhoGDI, confirming that PLPPR1 associates with RhoGDI and this
298 interaction is independent of the C-terminus (Fig. 7A).

299 Inactive RhoA (bound to GDP) is tightly sequestered by RhoGDI in the cytosol
300 (Ellerbroek et al., 2003; Garcia-Mata et al., 2011; Michaelson et al., 2001; Sabbatini and
301 Williams, 2013; Takahashi et al., 1997; Yamashita and Tohyama, 2003). LPA stimulation
302 results in the displacement of RhoA from RhoGDI. This allows RhoA to disengage GDP, bind
303 GTP and become activated (Kranenburg et al., 1997; Yoshioka et al., 1999). Therefore, to
304 determine how overexpression of PLPPR1 would affect the RhoGDI – RhoA interaction after
305 LPA treatment, Neuro2a cells transfected with EGFP or EGFP-PLPPR1 were exposed to either
306 FAFBSA, serum or LPA. RhoGDI was immunoprecipitated and immunoblot analysis of RhoA
307 was performed. We found that the interaction between RhoA and RhoGDI was disrupted in
308 EGFP-transfected cells after treatment with either serum or LPA, as expected. However, the
309 interaction of RhoGDI for RhoA was maintained in cells overexpressing PLPPR1 even after

310 serum or LPA treatment (Fig. 7B). Immunoblot analysis of GFP expression showed that protein
311 expression levels did not change between treatment conditions (Fig. 7B).
312 Like RhoA, Rac1 activation is regulated by RhoGDI (Boulter et al., 2010;
313 DerMardirossian et al., 2004). We therefore assessed the effects of PLPPR1 overexpression on
314 the affinity of RhoGDI for Rac1 after LPA treatment. Neuro2a cells transfected with EGFP or
315 EGFP-PLPPR1 were exposed to either FAFBSA, serum or LPA. RhoGDI was
316 immunoprecipitated and immunoblotting was performed to detect Rac1 levels. Our results show
317 that, like RhoA, the interaction between RhoGDI and Rac1 was disrupted by LPA treatment in
318 cells expressing EGFP, however, this interaction was maintained in cells overexpressing
319 PLPPR1 (Fig. 7B). Altogether, these results demonstrate that PLPPR1 modulates LPA induced
320 activation of RhoA and Rac1, via its association with RhoGDI.
321
322 **Co-expression of PLPPR1 and CA Rac1 reverts PLPPR1 induced morphological change**
323 Rac1 activation is essential to lamellipodial formation (Ehrlich et al., 2002; Kozma et al.,
324 1997; Somanath and Byzova, 2009). Typical membrane ruffling lamellipodia were found absent
325 in cells overexpressing PLPPR1 (Fig. 4A). Therefore, given the possibility that PLPPR1 may
326 regulate Rac1 activity, we examined the morphology of cells expressing dominant negative (DN)
327 Rac1 T17N, constitutively active (CA) Rac1 G12V and cells co-expressing PLPPR1 with CA
328 Rac1. We observed that expression of DN Rac1 caused a morphological change, similar to the
329 "trailing fibers" observed in cells overexpressing PLPPR1 (Fig. 8A). Interestingly, co-expression
330 of CA Rac1 with PLPPR1 was able to revert the morphological change induced by PLPPR1
331 (Fig. 8A).
332 To confirm the effect of PLPPR1 on Rac1 activation, DN Rac1 and CA Rac1 were
333 expressed in Neuro2a cells and active Rac1 bound to GTP was immunoprecipitated using PAK-
334 PBD beads. Basal levels of Rac1-GTP were near zero in Neuro2a cells transfected with EGFP,
335 as well as in cells overexpressing PLPPR1 and DN Rac1 (Fig. 8B, C). As expected, there were

336 high levels of active Rac1 in cells expressing CA Rac1, however, co-expression of CA Rac1
337 with PLPPR1 significantly reduced active Rac1 (Fig. 8B, C), confirming that PLPPR1 modulates
338 Rac1 activation.

339 Arp2/3 is an actin nucleating and crosslinking complex that acts downstream of Rac1
340 and is essential to actin assembly and lamellipodia formation (Lai et al., 2008; Machesky and
341 Hall, 1997; Machesky and Insall, 1998; Wu et al., 2012). Therefore, we examined Arp2/3 in cells
342 overexpressing PLPPR1 using STED microscopy. Results show that while Arp2/3 was localized
343 to the actin-rich lamellipodia and exhibited a more diffuse cytoplasmic distribution in cells
344 transfected with EGFP, cells overexpressing PLPPR1 displayed a compact aggregation of
345 Arp2/3 (Fig. 8D), suggesting a disruption in Arp2/3 localization. Together, these results
346 demonstrate a regulatory function for PLPPR1 in Rac1 activation.

347

348 **DISCUSSION**

349 The PLPPR family of proteins were initially identified as “Plasticity-Related Genes” due
350 to their upregulation in sprouting axons (Brauer et al., 2003). PLPPR1 expression levels
351 correlate with axon growth and remodeling after kainic acid treatment in the hippocampus
352 (Savaskan et al., 2004). Additionally, PLPPR1 was identified in a screen for molecules that
353 promote regeneration after spinal cord injury (Fink et al., 2017). More recently, the PLPPR
354 family of proteins have been implicated in the regulation of neurogenesis and neuronal
355 migration (Khalaf-Nazzal et al., 2017; Lyons et al., 2010; Pfurr et al., 2017). Exogenous
356 expression studies of PLPPR1 in cultured cells demonstrate that the major phenotype is the
357 induction of filopodia in many different cell types (Broggini et al., 2016; Velmans et al., 2013; Yu
358 et al., 2015). The mechanism of action by which PLPPR1 induces these morphological changes
359 has been a subject of intense speculation.

360 Here, we demonstrate that PLPPR1 modulates the RhoA-ROCK signaling pathway. We
361 show that through association with RhoGDI, PLPPR1 may prevent GTP loading by stabilizing

362 the interaction between RhoGDI and GDP bound RhoA and Rac1. This stabilization results in
363 reduced RhoA and Rac1 activity, leading to alterations in cytoskeletal dynamics. This explains
364 the effect of PLPPR1 on cell adhesion and consequently cell migration enabling PLPPR1 to
365 overcome the inhibitory activity of CSPGs and LPA on neurite outgrowth (Fig. 9).

366 The PLPPR family of proteins share sequence and structural homology with the lipid
367 phosphate phosphatase family (LPP), and are characterized by six transmembrane domains
368 with intracellular N-terminal and C-terminal domains (Brauer and Nitsch, 2008; Strauss and
369 Brauer, 2013). This homology to lipid phosphatases and the discovery that overexpression of
370 PLPPR4 could attenuate LPA-induced axon collapse (Brauer et al., 2003), provided support for
371 the hypothesis that PLPPR signaling was through extracellular lipid phosphatase activity.
372 However, the PLPPR proteins lack key amino acid residues critical to the phosphatase activity
373 of the LPP protein family and are not known to exhibit any phosphatase activity (Strauss and
374 Brauer, 2013), thus, other signaling pathways have been suggested.

375 In addition to attenuating LPA-induced axon collapse, overexpression of PLPPR1 can
376 reduce the inhibitory response to myelin (Broggini et al., 2016), and here, we show a similar
377 response to CSPGs. Each of these guidance cues are thought to signal through activation of the
378 RhoA GTPase (Alabed et al., 2006; Ohtake et al., 2016) and reducing RhoA activity with C3
379 exoenzyme attenuates their inhibitory actions, as does inhibition of the downstream effector,
380 Rho kinase, ROCK (Dergham et al., 2002; Fournier et al., 2003). Here, we demonstrate that
381 overexpression of PLPPR1 reduced RhoA activation in response to LPA treatment. This is
382 similar to the effect of its close homolog, PLPPR5, on RhoA activation by LPA (Broggini et al.,
383 2010). Furthermore, we confirmed the modulatory effect of PLPPR1 on RhoA activation of
384 ROCK targets, MLC, MYPT1 and the ERM proteins. A previous study also implicated PIP5K, a
385 protein kinase downstream of RhoA, as being altered by PLPPR1 expression (Broggini et al.,
386 2016).

387 RhoA activation is controlled by regulatory proteins such as the GEFs, that catalyze the
388 exchange of GDP for GTP, and the GDIs, that sequester RhoA in the cytosol, preventing its
389 translocation to the plasma membrane and thus, its activation (Bokoch et al., 1994; Dovas and
390 Couchman, 2005; Hodge and Ridley, 2016). We identified RhoGDI as a possible binding target
391 for PLPPR1 in a proteomic screen for interacting proteins (Yu et al., 2013), and we have
392 confirmed this interaction by co-immunoprecipitating PLPPR1 with RhoGDI. Without stimulation,
393 RhoA-GDP is tightly bound to RhoGDI (Boulter et al., 2010; Hodge and Ridley, 2016;
394 Tkachenko et al., 2011). Upon LPA treatment, this interaction is disrupted, permitting RhoA to
395 translocate to the plasma membrane and become activated. We have demonstrated here that
396 overexpression of PLPPR1 maintains the interaction of RhoA with RhoGDI after LPA treatment
397 suggesting that PLPPR1 may play a role in stabilizing the RhoA-RhoGDI complex, thereby,
398 preventing the RhoA GDP exchange for GTP and its subsequent activation.

399 RhoGDI is known to regulate the activity of the small GTPases, Rac1 and Cdc42.
400 Expression of DN Rac1 prevents GTP loading, resulting in a failure to form proper lamellipodia
401 (Ehrlich et al., 2002; McCarty et al., 2005). Interestingly, we show that expression of DN Rac1
402 exhibits a similar morphological change as overexpression of PLPPR1 in Neuro2a cells. Our
403 results also show that co-expression of PLPPR1 with CA Rac1 reverts this morphological
404 change in Neuro2a cells. This is consistent with our results that demonstrate a stable Rac1-
405 RhoGDI complex in cells overexpressing PLPPR1, suggesting a modulatory effect on Rac1
406 activity.

407 The formation of membrane protrusions by exogenous expression of PLPPR1 has been
408 shown to be independent of Cdc42, Arp2/3 and the EnA/VASP proteins, suggesting that the
409 PLPPR1 has no modulatory effect on Cdc42 (Sigal et al., 2007). Additionally, co-expression of
410 PLPPR1 with dominant negative Cdc42 or with WASP-CRIB, which recruits and activates
411 Arp2/3, did not reverse the morphological change induced by PLPPR1 overexpression (Sigal et
412 al., 2007). It is noteworthy that the nucleation of actin filaments by Arp2/3 complex is also driven

413 by WAVE, downstream of Rac1 activation (Chen et al., 2017; Lai et al., 2008). Therefore, while
414 Arp2/3 may not be required to induce membrane protrusions, it still remains that localization of
415 Arp2/3 is disrupted in cells overexpressing PLPPR1 and this may be a direct consequence of
416 altered Rac1 activity.

417 The PLPPR proteins are similar in their N-terminal domains, with significant divergence
418 in their intracellular C-terminal regions (Brauer and Nitsch, 2008). The C-terminal domain of
419 PLPPR1 is important for the induction of membrane protrusions (Broggini et al., 2016; Yu et al.,
420 2015), likely due to the inability of PLPPR1 lacking its C-terminus, to be transported to the cell
421 membrane (Yu et al., 2015). This domain is also the site of the change in phosphorylation by
422 CSPGs (Yu et al., 2013), and has been reported to modulate Ras activity by interacting with
423 RasGRF1 (Broggini et al., 2016). However, our data show that the PLPPR1 C-terminal domain
424 is dispensable for its ability to overcome the inhibitory activity of CSPGs and LPA and is not
425 necessary for its association with RhoGDI, suggesting that while the C-terminal domain of
426 PLPPR1 may be important for the induction of membrane protrusions, it is not essential to its
427 modulation of RhoA and Rac1 activity. Interestingly, the C-terminal of PLPPR5, the closest
428 family member to PLPPR1, has also been reported to be essential for formation of protrusions
429 (Broggini et al., 2010). Whether there is a similar interaction of PLPPR5 with RhoGDI remains
430 an open question.

431 PLPPR1 overexpression ultimately results in increased adhesion and decreased
432 migration of cells on a fibronectin substrate. Cell migration is an integrated process that involves
433 the spatio-temporal coordination of actin cytoskeletal dynamics with focal adhesion turnover
434 (Gardel et al., 2010; Le Clainche and Carlier, 2008; Webb et al., 2002). Cellular adhesion to
435 fibronectin is mediated through the engagement and activation of integrins, which then promote
436 the establishment of focal adhesion complexes that are also regulated by the activity of the
437 Rac1 and RhoA GTPases (Nobes and Hall, 1995; Rottner et al., 1999; Sinnett-Smith et al.,
438 2001). Mechanical tension promotes the growth and maturation of focal adhesions that is driven

439 by RhoA mediated myosin II activity (Pasapera et al., 2010) and this is required for the
440 coordinated propulsive force that enables cell migration (Gardel et al., 2010; Lauffenburger and
441 Horwitz, 1996). Several studies have demonstrated that inhibition of Rho-ROCK activity
442 prevents the maturation of focal adhesions (Burridge and Guilluy, 2016; Sawada et al., 2002;
443 Sinnett-Smith et al., 2001). Therefore, it is conceivable that the reduced RhoA activity and the
444 nascent focal adhesion complexes that persists in cells overexpressing PLPPR1 may account
445 for the decrease in cell migration. This is consistent with the increase in phosphorylation of
446 paxillin and FAK observed in these cells, given that FAK mediated phosphorylation of paxillin
447 plays a role in the assembly, turnover and stability of focal adhesions complexes (Lawson et al.,
448 2012; Pasapera et al., 2010; Turner, 2000; Webb et al., 2004; Zaidel-Bar et al., 2007). It is
449 essential to note that while increased phosphorylation of paxillin and FAK is observed in cells
450 overexpressing PLPPR1, this does not imply direct kinase activity on paxillin and FAK by
451 PLPPR1 but suggests an indirect effect on the phosphorylation of paxillin and FAK.
452 Another member of the PLPPR family, PLPPR4, mediates cell adhesion through
453 activation of ß1-integrins (Liu et al., 2016). Through the calmodulin-binding domain (CBD) in its
454 long cytoplasmic C-terminal tail consisting of ~400 a min o acid residues that is unique to this
455 PLPPR family member alone, PLPPR4 interacts with protein phosphatase 2A (PP2A) to
456 organize the assembly of an integrin adhesome consisting of talin, paxillin and src, thereby
457 stimulating activation of ß1-integrin (Liu et al., 2016). While PLPPR1 lacks the key motifs in its
458 C-terminal domain that is characteristic of PLPPR4, and we have demonstrated that the
459 increased cell adhesion observed in PLPPR1 is independent of its C-terminal domain, it still
460 remains that PLPPR1 may mediate activation of ß1-integrins through other means to increase
461 cell adhesion. Additionally, there is evidence that PLPPR1 may associate with ß1-integrin (Yu et
462 al., 2013), however, this putative interaction is yet to be confirmed.
463 Mesenchymal type cell migration is characterized by increased focal adhesion sites at
464 the leading edge of the cell and an adhesive “pulling” during migration, causing parts of the

465 membrane protrusions to remain adhered to the ECM as the cell migrates away (Friedl and
466 Wolf, 2010; Schmidt and Friedl, 2010). We found that cells transfected with PLPPR1 did not
467 disengage from the substrate during migration, leaving long plasma membrane extensions that
468 we have termed "trailing fibers". The presence of these "trailing fibers" suggest an inability of the
469 cells to detach from the substrate due to increased adhesion.

470 While overexpression of PLPPR1 increases cell adhesion, biological functions, such as
471 alteration of neurogenesis (Pfurr et al., 2017), neuronal migration (Khalaf-Nazzal et al., 2017)
472 and regulation of axonal growth (Fink et al., 2017), have been inferred from experiments using
473 genetic screening approaches. Determining the role of PLPPR1 would require the ability to
474 silence PLPPR1 mRNA and confirm the knock-down using protein-detection techniques.
475 Unfortunately, there are no reliable commercial antibodies to detect this protein, thus,
476 preventing these studies.

477 Taken together, our results provide evidence for a novel signaling mechanism of
478 PLPPR1 – the modulation of RhoA and Rac1 activity by interaction with RhoGDI. As its original
479 name, Plasticity-Related Gene protein 3, infers, PLPPR1 plays a role in mediating plasticity in
480 response to extracellular cues, through modulation of the RhoA – ROCK signaling pathway via
481 its association with RhoGDI. This mechanism serves as a potential explanation for the ability of
482 PLPPR1 to overcome CSPG and myelin-mediated inhibition of neurite outgrowth to promote
483 axon regeneration after injury.

484

485 **MATERIALS AND METHODS**

486

487 **Plasmid construction**

488 DNA constructs: The mApple-FTR-940 (F-tractin) was originally from Michael Davidson's
489 laboratory (plasmid # 54902, Addgene, Cambridge, MA). pEGFP-Rac1 G12V and pEGFP-Rac1
490 T17N were both obtained from Clontech (Mountain view, CA). mApple-paxillin was kindly

491 provided by Clare Waterman (National Institutes of Health, Bethesda, MD). PLPPR1 cDNA was
492 amplified from a mouse brain cDNA library. Full-length PLPPR1 (amino acids 1–325) and
493 PLPPR1 lacking the last 43 amino acid residues of the C-terminal region (PLPPR1ΔC43, amino
494 acids 1–282) were inserted into the pEGFP-C1 vector with the EGFP tag fused to the N-
495 terminus of PLPPR1 cDNA using the In-Fusion cloning system (Clontech, Mountain View, CA).
496 A construct expressing C-terminal HA-tagged PLPPR1 (PLPPR1–HA) was kindly provided by
497 Andrew J. Morris (University of Kentucky, Lexington, KY) (Sigal et al., 2007). The
498 oligonucleotide primer pairs used were as follows:
499 PLPPR1 SalIfusC1F: 5'GAATTCTGCAGTCGACGCCACCATGGCTGTAGAAAACAACACTCA3'
500 PLPPR1 SacIIfusC1R:
501 5'GTGGATCCCGGGCCCGCGGTCAGGTGACTTCGGTCATGGAGGCG3'
502 PLPPR1ΔC43aaSacIIfusC1R:
503 5'GTGGATCCCGGGCCCGCGGTCAGGTTCCTCTGAAGTTATGAA3'
504

505 **Cell culture and transfection**

506 All animal procedures were performed in accordance with protocols approved by the
507 Institutional Animal Care and Use Committee (IACUC) at the National Institutes of Health.
508 Timed pregnant C57BL/6J mice were housed in a pathogen free facility with free access to food
509 and water under a standard 12h light/dark cycle.

510 Primary hippocampal neurons were isolated from embryonic day 18 – 20 C57BL/6J
511 pregnant mice and transfected with 1μg of either EGFP, EGFP-PLPPR1 or EGFP-
512 PLPPR1ΔC43 plasmid DNA per well using the 96-well shuttle Amaxa Nucleofector™ kit,
513 program CA-138 (Lonza, Walkersville, MD). Neurons were grown in Neurobasal media
514 supplemented with antibiotics (penicillin/streptomycin), glutamax, B27 (ThermoFisher Scientific,
515 Waltham, MA) and 2mM potassium chloride (KCl) for 48h.

516 Neuro2a cells were maintained in DMEM supplemented with penicillin/streptomycin
517 antibiotics and 10% fetal bovine serum (FBS). Twenty-four hours after plating, cells were
518 transfected with either EGFP or EGFP-PLPPR1 or EGFP-PLPPR1ΔC43, using Avalanche
519 Omni® transfection reagent (EZ Biosystems, College Park, MD).
520 For CSPG treatment and neurite outgrowth analysis, primary hippocampal neurons were
521 plated onto glass coverslips coated with either poly-l-lysine (PLL) or a soluble CSPG mix
522 containing neurocan, phosphacan, versican, and aggrecan isolated from embryonic chicken
523 brain (CC117 Millipore, Billerica, MA). Neurons were subsequently immunostained for anti-βIII
524 tubulin (Sigma Aldrich, St. Louis, MO) and imaged using a Nikon Eclipse Microscope with a
525 60×/1.4 NA oil immersion objective lens. Neurite outgrowth analysis was performed using the
526 NeuronJ plugin of ImageJ.
527 All cell culture plates (Corning, Corning NY), 6-well (3506), 12-well (3512), 24-well
528 (3527), 48-well (3548), MatTek dishes (35mm petri dish with 14mm microwells, No. 1.5, MatTek
529 Corporation, Ashland, MA) and Lab-Tek™ culture II chamber slides, (155382) (ThermoFisher
530 Scientific, Waltam, MA) were coated with 10μg/ml fibronectin (Millipore, Billerica, MA), unless
531 otherwise indicated, and incubated overnight at 4˚C. Excess fibronectin was rinsed off by
532 washing 3 times with Phosphate buffered saline (PBS).
533
534 **Immunocytochemistry**
535 Transfected Neuro2a cells were fixed in 4% PFA, 48h after plating and 24h after
536 transfection. Cells were briefly rinsed in PBS and incubated in blocking buffer (0.3% Triton X-
537 100 in PBS, supplemented with 10% normal goat serum, NGS) for 1h and then with primary
538 antibody diluted in 0.3% Triton X-100 in PBS, supplemented with 2.5% NGS. Cells were
539 washed in PBS and then incubated with secondary antibody diluted in 0.3% Triton X-100 in
540 PBS, supplemented with 2.5% NGS. See table for dilutions and source of antibodies. Cells were
541 then washed in PBS and then mounted with DAPI diluted in Fluoromount (Sigma-Aldrich). All

542 phalloidin (ThermoFisher Scientific, Waltam, MA) staining was performed as previously
543 described (Yu et al., 2015).
544 For STED microscopy, cells were mounted in prolong diamond mounting media
545 (ThermoFisher Scientific, Waltam, MA) and imaged on a Leica SP8 STED 3X/Confocal
546 Microscope using 100×/1.4 oil immersion objective lens (Leica Microsystems, Buffalo Grove, IL).
547 All other imaging was performed on a Zeiss 780 LSM confocal microscope using 63×/1.4 oil
548 immersion objective lens.
549

550 **Live cell imaging**

551 All live cell imaging was conducted on microscopes equipped with a heated stage at
552 37˚C and 5% CO_2 on either a Nikon A1R microscope (Nikon Instruments Inc., Melville, NY), a
553 Zeiss 780 LSM confocal microscope (Carl Zeiss, Thornwood, NY) or an Delta Vision OMX
554 microscope (GE, Malborough, MA).
555

556 **Cell migration assay**

557 Neuro2a cells transfected with either EGFP or EGFP-PLPPR1 were plated in Lab-Tek
558 culture chamber slides coated with fibronectin. Time lapse images were acquired for 10h at the
559 rate of 1 frame/10 min on a Nikon A1R microscope using a 10×/0.45 NA objective lens. Cell
560 migration was analyzed by tracking each transfected cell, using the middle of each cell body as
561 the point of reference. The distance travelled was determined using NIS Elements software
562 (Nikon Instruments Inc., Melville, NY).
563

564 **Cell adhesion assay**

565 Neuro2a cells transfected with either EGFP, EGFP-PLPPR1 or EGFP-PLPPR1ΔC43
566 were plated in T75 culture flasks and detached with 5mM EDTA. Cells were replated in a 48-
567 well plate coated with fibronectin at a density of 2.0×10^5 cells per well. Cells were allowed to

568 adhere for 1h after plating and then washed briefly with DMEM culture media every 15 min
569 thereafter. Fluorescence detection was performed on a SpectraMax M3 microplate reader
570 (Molecular Devices, San Jose, CA). The cell density of adherent transfected cells was
571 determined by fluorescence using the Softmax Pro7 software (Molecular Devices, San Jose,
572 CA). Cell adhesion was calculated as the percentage of transfected cells that persists after each
573 wash, from unwashed transfected cells. Cells were subsequently fixed in 4% PFA, rinsed twice
574 in PBS and stained with DAPI. Images were acquired on a Nikon A1R microscope using a
575 10×/0.45 NA oil objective lens.
576 For the detachment assay, Neuro2a cells were plated on a 12-well plate coated with
577 fibronectin and transfected with either EGFP or EGFP-PLPPR1, 24 h after plating. After another
578 24h, cells were briefly washed with DMEM culture media to remove serum and subsequently
579 treated with Trypsin-EDTA diluted in DMEM (1:10) with increasing time intervals. Cells were
580 then rinsed with PBS, fixed with 4% PFA and stained with DAPI. 10 × 10 tiled images were
581 acquired on a Zeiss 780 LSM confocal microscope using a 10×/0.45 NA dry objective lens.
582
583 **Interference reflection microscopy**
584 Neuro2a cells transfected with either EGFP or EGFP-PLPPR1 were fixed with 4% PFA
585 for 15 min , 24h post transfection. Images were acquired with a Zeiss 780 LSM confocal
586 microscope using a 63×/1.4 NA oil immersion objective lens. Single-frame TIFF images were
587 extracted from TIFF stacks and processed using ImageJ. The area of each cell was traced from
588 bright field images to obtain an ROI (region of interest). The image was then rescaled to an 8-bit
589 scale of 0–255 based on pixel intensity values that fell within histogram bins exceeding 5%
590 of the mean histogram bin height. A band pass filter was applied based on convolution with a
591 41 × 41pixel kernel. The histogram was then stretched again based on a 5% cut-off of the
592 mean values. A binary threshold was fixed by selecting pixel intensities above 90 on the 0 – 255

593 scale. The image was then inverted and the number of pixels above threshold was divided by
594 the area of the ROI to determine intensity. A color map 'Gem' was used to display higher
595 intensity pixels as blue and lower intensity as orange which represent stronger and weaker
596 adhesions respectively. For quantification, the area of each cell was traced from bright field
597 images to obtain the region of interest. A threshold was applied to the IRM image of the same
598 cell and the number of pixels above threshold was divided by the ROI to calculate the area of
599 cell attachment.

600 To measure the size of focal adhesion (FA) contacts, Neuro2a cells were plated on
601 MatTek dishes at a density of 2×10^4 cells and transfected with either EGFP or EGFP-PLPPR1.
602 Cells were fixed and stained with anti-paxillin antibody. Images were acquired using TIRF
603 microscopy on an inverted TIRF OMX Delta Vision microscope system using a 60×/1.49 NA
604 TIRF objective lens. Counting of FAs in single cells (n = 10 cells) was done after noise removal
605 by thresholding and applying a size constraint to FAs using ImageJ software.

606

607 **Actin turnover analyzed by FRAP**

608 Neuro2a cells, plated on glass-bottom MatTek dishes coated with fibronectin, were co-
609 transfected with F-tractin (mApple-FTR-940) and either EGFP or EGFP-PLPPR1. FRAP
610 experiments were conducted on a Nikon A1R microscope using a 60×/1.4 NA oil objective lens.
611 A ROI was selected from the leading edge of transfected cells and a 564 nm laser at 20%
612 intensity was used as a pre-bleaching signal for F-tractin. The ROI was subsequently
613 photobleached by three lasers at 458nm, 564nm and 633nm, all set at 100% intensity. The
614 post-bleaching acquisition was carried out at 60 frames at a rate of 1 frame/0.6s. The
615 fluorescence intensity was determined at every time point and automatically generated by NIS
616 Elements software. Images were corrected for photobleaching and the fluorescence intensity of
617 the ROI for each frame was normalized to the average initial intensity of pre-bleaching frames
618 and to the area of the bleached cell. The fluorescence intensity for the pre-bleaching frames

619 was calculated as the average fluorescence intensity in the first 5 frames, F_{pre}. The value, F_0,
620 was designated as the average fluorescence intensity of the 8th frame after the photobleaching
621 phase that occurred in the 6th and 7th frames. Individual plots for each experiment was fitted to a
622 model function. The fluorescence recovery of F-tractin was best fitted by a single-exponential
623 function (double exponential function did not significantly improve the quality of the fit) using
624 Matlab, revealing the presence of mobile actin fractions with different recovery kinetics. The
625 following model was applied:

626 $$F(t) = A[1 - exp(-Bt)]$$

627 Where: A is the percentage of mobile fraction of actin and B is the time constant of fluorescence
628 recovery. A and B were obtained from the fitted curve. The mean ± SEM was calculated for the
629 percentage of fluorescence recovery and the time constant for each condition. The final graphs
630 show the fluorescence recovery, mobile fraction of monomeric actin and $t_{1/2}$ which indicates the
631 time it took for F-actin polymerization.

632

633 **LPA treatment**

634 Serum starved Neuro2a cells transfected with either EGFP or EGFP-PLPPR1 were
635 treated with fatty-acid free bovine serum albumin, FAFBSA, (Sigma Aldrich, St. Louis, MO), or
636 Lysophosphatidic acid, LPA (Cayman Chemical, Ann Arbor, MI) diluted in FAFBSA. Time lapse
637 images were acquired on a Nikon A1R microscope with a 20×/0.75 dry objective lens with no
638 time delay between frames for 20 min . Cell response was calculated as percentage of the total
639 transfected cell count that retracted their neurites or underwent cell rounding.

640

641 **Western blot assay**

642 Neuro2a cells seeded at a density of 4×10^5 cells/well in a 6-well culture dish were
643 transfected with either EGFP or EGFP-PLPPR1. Cells were either serum-starved for 16 – 18h
644 or maintained in DMEM supplemented with 10% FBS. Serum starved cells were then treated

645 with either FAFBSA, 10% serum or increasing concentrations of LPA: 4, 8 and 16μM for 2 min .
646 Media was gently but completely removed from all cells and rinsed once with warmed PBS. Cell
647 lysates were prepared in 2× SDS cell lysis buffer and clarified by centrifugation. Protein
648 quantitation was performed using Ionic Detergent Compatibility Reagent for Pierce™ 660nm
649 Protein Assay Reagent (ThermoFisher Scientific, Waltam, MA) by BCA method. Equal
650 concentration of proteins (20μg/lane) were separated on SDS-PAGE and transferred onto a
651 polyvinylidene difluoride (PVDF) membrane (Bio-Rad Laboratories, Inc. Hercules, CA).
652 Membranes were blocked for 1h in 5% nonfat dried milk in either 0.1% Tween20 in PBS (PBST)
653 or 0.1% Tween20 in 10mM Tris–HCl pH 7.5 (TBST) or blocked in 5% BSA in TBST. Membranes
654 were incubated with primary antibodies overnight at 4˚C, washed in either PBST or TBST and
655 subsequently incubated with secondary antibody for 30 min . Antigen–antibody complexes were
656 detected with KPL LumiGlo chemiluminescent substrate (Seracare, Milford, MA). See Table 1
657 for source and dilutions for all primary and secondary antibodies used.
658
659 **Co-immunoprecipitation assay**
660 Neuro2a cells were seeded at a density of 4 × 10^5 cells/well in a 6-well culture dish and
661 transfected with either EGFP, EGFP-PLPPR1 or EGFP-PLPPR1ΔC43. Cells were harvested,
662 washed twice in ice-cold PBS and then resuspended in ice-cold cell lysis buffer (10mM Tris pH
663 7.5, 150mM NaCl, 0.5mM EDTA, 1% NP-40 supplemented with protease inhibitor cocktail set V
664 EDTA free (Millipore, Billerica, MA) and phosphatase inhibitors (Thermo Fisher Scientific,
665 Waltham, MA). Cell lysates were cleared and then incubated with GFP-Trap MA beads as
666 instructed in ChromoTek GFP-Trap® MA immunoprecipitation kit (ChromoTek Inc., Hauppauge,
667 NY). Cell lysates were subsequently washed twice in dilution buffer (10mM Tris-HCl pH 7.5,
668 150mM NaCl, 0.5mM EDTA, 0.5% NP-40 supplemented with protease and phosphatase
669 inhibitors) and then once in wash buffer (10mM Tris-HCl pH 7.5, 500mM NaCl, 0.5mM EDTA,
670 0.5% NP-40 supplemented with protease and phosphatase inhibitors). Protein was eluted and

671 subjected to SDS-PAGE as described above.

672 To immunoprecipitate RhoGDI, transfected cells were rinsed in warmed PBS, harvested
673 in cell lysis buffer (20mM Tris pH 7.5, 150mM NaCl, 0.5mM EDTA, 1% NP-40 supplemented
674 with protease and phosphatase inhibitors) and precleared with rabbit IgG serum and Protein G
675 agarose beads (Seracare, Milford, MA). Samples were subsequently incubated with primary
676 antibody overnight at 4˚C and then incubated with Protein G agarose beads for 1h at 4˚C.
677 Samples were washed twice in dilution buffer (20mM Tris pH 7.5, 150mM NaCl, 0.5mM EDTA,
678 0.5% NP-40 supplemented with protease and phosphatase inhibitors) and once in wash buffer
679 (20mM Tris pH 7.5, 500mM NaCl, 0.5mM EDTA, 0.5% NP-40 supplemented with protease and
680 phosphatase inhibitors). Protein was eluted and subjected to SDS-PAGE as described above.
681

682 **RhoA and Rac1 pull-down assay**

683 Serum starved Neuro2a cells transfected with either EGFP or EGFP-PLPPR1 were
684 treated with either FAFBSA, 10% serum or 16μM LPA. Briefly, cells were rinsed with warmed
685 PBS and cell lysates prepared in cell lysis buffer as instructed and provided by the RhoA or
686 Rac1 pull-down instruction manual and kit (Cytoskeleton, Inc. Denver, CO). Protein quantitation
687 was performed by BCA method and 600μg of protein was incubated with 50μg Rhotekin-RBD
688 beads for RhoA pull-down or with 10μg of PAK-PBD beads for Rac1 pull-down at 4˚C for 1h.
689 Complexes were washed in wash buffer provided in the pull-down kit and protein was eluted in
690 2× SDS sample buffer and SDS-PAGE performed as described above.
691

692 **Statistical analysis**

693 All analyses were performed using GraphPad Prism software version 7 (GraphPad
694 Software, La Jolla, CA). Data was analyzed by unpaired Student's *t* tests, one-way ANOVA or
695 two-way ANOVA with Welch's correction or Tukey's post-hoc multiple comparison test to
696 determine significance. Normality of the distribution of the data was tested with Kolmogorov–

697 Smirnov normality tests using the column statistics function of GraphPad Software. All tests
698 were two-tailed with significance indicated as follows: *p<0.05; **p<0.01; ***p<0.001;
699 ****p<0.0001. Unless otherwise specified, values represent the means ± SEM. All experiments
700 were repeated independently at least three times.
701

Primary Antibodies	**Dilution**	**Source**
Mouse anti-βIII tubulin	1:1000	Sigma Aldrich (SAB4700544)
Chicken anti-GFP	1:2000	Abcam (ab13970)
Rabbit anti-phospho-myosin light chain II (Ser19)	1:1000	Cell Signaling Technology (3671)
Rabbit anti-phospho-myosin light chain phosphatase I (Thr853)	1:1000	Cell Signaling Technology (4563)
Rabbit anti-phospho-GSK3β (Tyr216)	1:1000	Abcam (ab75745)
Rabbit anti-pERM	1:1000	Cell Signaling Technology (3141)
Rabbit anti-phospho-AKT (Ser473)	1:1000	Cell Signaling Technology (9271)
Rabbit anti-phospho-Tau (Ser396)	1:1000	Abcam (ab109390)
Rabbit anti-myosin light chain II	1:1000	Cell Signaling Technology (3672)
Rabbit anti-myosin light chain phosphatase I	1:1000	Cell Signaling Technology (2634)
Rabbit anti-GSK3β	1:1000	Cell Signaling Technology (27C10)
Rabbit anti-ERM	1:1000	Cell Signaling Technology (3142)
Rabbit anti-AKT	1:1000	Cell Signaling Technology (4685)
Rabbit anti-RhoGDI	1:1000	ThermoFisher Scientific (51-1000Z)
Anti-p34-Arc/ARPC2	1:100	Sigma Aldrich (07-227)
Mouse anti-Rac1	1:500	Cytoskeleton, Inc. (ARC03)
Mouse anti-Tau	1:2000	ThermoFisher Scientific (MA5-12808)
Mouse anti-RhoA	1:500	Cytoskeleton, Inc. (ARH03)

Mouse anti-β-actin	1:4000	Sigma Aldrich (A1978)
Rabbit anti-phospho-paxillin (Tyr31)	1:1000	ThermoFisher Scientific (44-720G)
Mouse anti-paxillin	1:1000	BD Biosciences (612405)
Rabbit anti-phospho FAK (Tyr576)	1:500	Epitomics (1700-1)
Rabbit anti-FAK	1:500	Epitomics (2103-1)

Secondary Antibodies	**Dilution**	**Source**
AlexaFluor 568, Goat anti-Mouse IgG	1:1000	Molecular Probes (A-11019)
Alexa Fluor 488, Goat anti-Chicken	1:1000	ThermoFisher Scientific (A-11039)
Goat anti-Chicken HRP	1:2000	Abcam (ab6877)
Veriblot for IP Detection Reagent (HRP)	1:4000	Abcam (ab131366)
Donkey anti-Rabbit IgG HRP-linked $F(ab')_2$ fragment	1:2000	Amersham-GE (NA9310)
Sheep anti-Mouse IgG HRP-linked $F(ab')_2$ fragment	1:2000 or 1:4000	Amersham-GE (NA9340)
Texas Red®-X phalloidin	1:500	ThermoFisher Scientific (T7471)

Online supplementary material

Fig. S1 shows cells overexpressing PLPPR1 resist trypsin detachment from the fibronectin substrate. Fig. S2 shows that the C-terminal domain of PLPPR1 is not essential to its ability to overcome CSPG inhibition of neurite outgrowth in primary hippocampal neurons. Fig. S3 shows that the C-terminal domain of PLPPR1 is not required to impede LPA induced neurite retraction and cell rounding. Fig. S4 shows that treatment of Neuro2a cells with LPA increases pERM levels and induces localization to the cell membrane in EGFP transfected cells, while pERM levels remain unchanged and localized in the cytosol in cells overexpressing PLPPR1. Fig. S5 shows that overexpression of PLPPR1 has no effect on phosphorylated levels of GSK3ß, Tau or

AKT after LPA treatment. Fig. S6 shows that without LPA stimulation, PLPPR1 has no effect on ROCK targets, MLC, MYPT1, pERM, including GSK3ß, Tau and AKT.

Acknowledgements

We wish to thank Daniela Malide and the NHLBI Light Microscopy Core facility for their help and guidance and Clare Waterman for materials provided.

This work was funded by the NIH Intramural Research Program.

The authors declare no competing financial interests.

Author contributions: C.A. Iweka, S. Tilve and H.M. Geller conceived the project. C.A. Iweka and S. Tilve performed all the experiments. C.A. Iweka, S. Tilve and H.M. Geller wrote the manuscript. All authors planned the experiments, analyzed and discussed the results and commented on the manuscript.

References

Alabed, Y.Z., E. Grados-Munro, G.B. Ferraro, S.H. Hsieh, and A.E. Fournier. 2006. Neuronal responses to myelin are mediated by rho kinase. *J. Neurochem.* 96:1616-1625. doi: 10.1111/j.1471-4159.2006.03670.x.

Amano, M., K. Chihara, K. Kimura, Y. Fukata, N. Nakamura, Y. Matsuura, and K. Kaibuchi. 1997. Formation of actin stress fibers and focal adhesions enhanced by Rho-kinase. *Science*. 275:1308-1311.

Baudhuin, L.M., K.L. Cristina, J. Lu, and Y. Xu. 2002. Akt activation induced by lysophosphatidic acid and sphingosine-1-phosphate requires both mitogen-activated protein kinase kinase and p38 mitogen-activated protein kinase and is cell-line specific. *Mol. Pharmacol.* 62:660-671. doi: 10.1124/mol.62.3.660.

738 Bellis, S.L., J.T. Miller, and C.E. Turner. 1995. Characterization of tyrosine
739 phosphorylation of paxillin in vitro by focal adhesion kinase. *J. Biol. Chem.* 270:17437-
740 17441.

741 Bokoch, G.M., B.P. Bohl, and T.H. Chuang. 1994. Guanine nucleotide exchange
742 regulates membrane translocation of Rac/Rho GTP-binding proteins. *J. Biol. Chem.*
743 269:31674-31679.

744 Boulter, E., R. Garcia-Mata, C. Guilluy, A. Dubash, G. Rossi, P.J. Brennwald, and K.
745 Burridge. 2010. Regulation of Rho GTPase crosstalk, degradation and activity by
746 RhoGDI1. *Nat. Cell Biol.* 12:477-483. doi: 10.1038/ncb2049.

747 Brauer, A.U., and R. Nitsch. 2008. Plasticity-related genes (PRGs/LRPs): a brain-
748 specific class of lysophospholipid-modifying proteins. *Biochim. Biophys. Acta*. 1781:595-
749 600. doi: 10.1016/j.bbalip.2008.04.004.

750 Brauer, A.U., N.E. Savaskan, H. Kuhn, S. Prehn, O. Ninnemann, and R. Nitsch. 2003. A
751 new phospholipid phosphatase, PRG-1, is involved in axon growth and regenerative
752 sprouting. *Nat. Neurosci.* 6:572-578. doi: 10.1038/nn1052.

753 Broggini, T., R. Nitsch, and N.E. Savaskan. 2010. Plasticity-related gene 5 (PRG5)
754 induces filopodia and neurite growth and impedes lysophosphatidic acid- and nogo-A-
755 mediated axonal retraction. *Mol. Biol. Cell*. 21:521-537. doi: 10.1091/mbc.E09-06-0506.

756 Broggini, T., L. Schnell, A. Ghoochani, J.M. Mateos, M. Buchfelder, K. Wiendieck, M.K.
757 Schafer, I.Y. Eyupoglu, and N.E. Savaskan. 2016. Plasticity Related Gene 3 (PRG3)
758 overcomes myelin-associated growth inhibition and promotes functional recovery after
759 spinal cord injury. *Aging (Albany N. Y.)*. 8:2463-2487. doi: 10.18632/aging.101066.

760 Burridge, K., and C. Guilluy. 2016. Focal adhesions, stress fibers and mechanical
761 tension. *Exp. Cell Res.* 343:14-20. doi: 10.1016/j.yexcr.2015.10.029.

762 Chen, B., H.T. Chou, C.A. Brautigam, W. Xing, S. Yang, L. Henry, L.K. Doolittle, T.
763 Walz, and M.K. Rosen. 2017. Rac1 GTPase activates the WAVE regulatory complex
764 through two distinct binding sites. *Elife*. 6. doi: 10.7554/eLife.29795.

765 Davies, S.J., D.R. Goucher, C. Doller, and J. Silver. 1999. Robust regeneration of adult
766 sensory axons in degenerating white matter of the adult rat spinal cord. *J. Neurosci.*
767 19:5810-5822.

768 DePasquale, J.A. 1998. Cell matrix adhesions and localization of the vitronectin
769 receptor in MCF-7 human mammary carcinoma cells. *Histochem. Cell Biol.* 110:485-
770 494.

771 Dergham, P., B. Ellezam, C. Essagian, H. Avedissian, W.D. Lubell, and L. McKerracher.
772 2002. Rho signaling pathway targeted to promote spinal cord repair. *J. Neurosci.*
773 22:6570-6577. doi: 10.1523/JNEUROSCI.22-15-06570.2002.

774 DerMardirossian, C., A. Schnelzer, and G.M. Bokoch. 2004. Phosphorylation of RhoGDI
775 by Pak1 mediates dissociation of Rac GTPase. *Mol. Cell*. 15:117-127. doi:
776 10.1016/j.molcel.2004.05.019.

777 Dovas, A., and J.R. Couchman. 2005. RhoGDI: multiple functions in the regulation of
778 Rho family GTPase activities. *Biochem. J.* 390:1-9. doi: 10.1042/BJ20050104.

779 Ehrlich, J.S., M.D. Hansen, and W.J. Nelson. 2002. Spatio-temporal regulation of Rac1
780 localization and lamellipodia dynamics during epithelial cell-cell adhesion. *Dev. Cell*.
781 3:259-270. doi: 10.1016/S1534-5807(02)00216-2.

782 Ellerbroek, S.M., K. Wennerberg, and K. Burridge. 2003. Serine phosphorylation
783 negatively regulates RhoA in vivo. *J. Biol. Chem.* 278:19023-19031. doi:
784 10.1074/jbc.M213066200.

785 Fang, X., S. Yu, J.L. Tanyi, Y. Lu, J.R. Woodgett, and G.B. Mills. 2002. Convergence of
786 multiple signaling cascades at glycogen synthase kinase 3: Edg receptor-mediated
787 phosphorylation and inactivation by lysophosphatidic acid through a protein kinase C-
788 dependent intracellular pathway. *Mol. Cell. Biol.* 22:2099-2110. doi:
789 10.1128/mcb.22.7.2099-2110.2002.

790 Fink, K.L., F. Lopez-Giraldez, I.J. Kim, S.M. Strittmatter, and W.B.J. Cafferty. 2017.
791 Identification of intrinsic axon growth modulators for intact CNS neurons after injury. *Cell*
792 *Rep.* 18:2687-2701. doi: 10.1016/j.celrep.2017.02.058.

793 Fournier, A.E., B.T. Takizawa, and S.M. Strittmatter. 2003. Rho kinase inhibition
794 enhances axonal regeneration in the injured CNS. *J. Neurosci.* 23:1416-1423. doi:
795 10.1523/JNEUROSCI.23-04-01416.2003.

796 Friedl, P., and K. Wolf. 2010. Plasticity of cell migration: a multiscale tuning model. *J.*
797 *Cell Biol.* 188:11-19. doi: 10.1083/jcb.200909003.

798 Garcia-Mata, R., E. Boulter, and K. Burridge. 2011. The 'invisible hand': regulation of
799 RHO GTPases by RHOGDIs. *Nat. Rev. Mol. Cell Biol.* 12:493-504. doi:
800 10.1038/nrm3153.

801 Gardel, M.L., I.C. Schneider, Y. Aratyn-Schaus, and C.M. Waterman. 2010. Mechanical
802 integration of actin and adhesion dynamics in cell migration. *Annu. Rev. Cell Dev. Biol.*
803 26:315-333. doi: 10.1146/annurev.cellbio.011209.122036.

804 Haemmerli, G., and P. Strauli. 1981. In vitro motility of cells from human epidermoid
805 carcinomas. A study by phase-contrast and reflection-contrast cinematography. *Int. J.*
806 *Cancer*. 27:603-610.

807 Hodge, R.G., and A.J. Ridley. 2016. Regulating Rho GTPases and their regulators. *Nat.*
808 *Rev. Mol. Cell Biol.* 17:496-510. doi: 10.1038/nrm.2016.67.

809 Hynds, D.L., and D.M. Snow. 1999. Neurite outgrowth inhibition by chondroitin sulfate
810 proteoglycan: stalling/stopping exceeds turning in human neuroblastoma growth cones.
811 *Exp. Neurol.* 160:244-255. doi: 10.1006/exnr.1999.7212.

812 Jain, A., S.M. Brady-Kalnay, and R.V. Bellamkonda. 2004. Modulation of Rho GTPase
813 activity alleviates chondroitin sulfate proteoglycan-dependent inhibition of neurite
814 extension. *J. Neurosci. Res.* 77:299-307. doi: 10.1002/jnr.20161.

815 Jalink, K., T. Eichholtz, F.R. Postma, E.J. van Corven, and W.H. Moolenaar. 1993.
816 Lysophosphatidic acid induces neuronal shape changes via a novel, receptor-mediated
817 signaling pathway: similarity to thrombin action. *Cell Growth Differ.* 4:247-255.

818 Kaneko-Kawano, T., F. Takasu, H. Naoki, Y. Sakumura, S. Ishii, T. Ueba, A. Eiyama, A.
819 Okada, Y. Kawano, and K. Suzuki. 2012. Dynamic regulation of myosin light chain
820 phosphorylation by Rho-kinase. *PLoS One*. 7:e39269. doi:
821 10.1371/journal.pone.0039269.

822 Khalaf-Nazzal, R., M.A. Stouffer, R. Olaso, L. Muresan, A. Roumegous, V. Lavilla, W.
823 Carpentier, I. Moutkine, S. Dumont, B. Albaud, N. Cagnard, H. Roest Crollius, and F.
824 Francis. 2017. Early born neurons are abnormally positioned in the doublecortin
825 knockout hippocampus. *Hum. Mol. Genet.* 26:90-108. doi: 10.1093/hmg/ddw370.

826 Kim, E.K., J.M. Park, S. Lim, J.W. Choi, H.S. Kim, H. Seok, J.K. Seo, K. Oh, D.S. Lee,
827 K.T. Kim, S.H. Ryu, and P.G. Suh. 2011. Activation of AMP-activated protein kinase is

828 essential for lysophosphatidic acid-induced cell migration in ovarian cancer cells. *J. Biol.*
829 *Chem.* 286:24036-24045. doi: 10.1074/jbc.M110.209908.

830 Kozma, R., S. Sarner, S. Ahmed, and L. Lim. 1997. Rho family GTPases and neuronal
831 growth cone remodelling: relationship between increased complexity induced by
832 Cdc42Hs, Rac1, and acetylcholine and collapse induced by RhoA and lysophosphatidic
833 acid. *Mol Cell Biol*. 17:1201-1211.

834 Kranenburg, O., M. Poland, M. Gebbink, L. Oomen, and W.H. Moolenaar. 1997.
835 Dissociation of LPA-induced cytoskeletal contraction from stress fiber formation by
836 differential localization of RhoA. *J. Cell Sci.* 110 (Pt 19):2417-2427.

837 Kranenburg, O., M. Poland, F.P. van Horck, D. Drechsel, A. Hall, and W.H. Moolenaar.
838 1999. Activation of RhoA by lysophosphatidic acid and Galpha12/13 subunits in
839 neuronal cells: induction of neurite retraction. *Mol. Biol. Cell*. 10:1851-1857. doi:
840 10.1091/mbc.10.6.1851.

841 Lai, F.P., M. Szczodrak, J. Block, J. Faix, D. Breitsprecher, H.G. Mannherz, T.E.
842 Stradal, G.A. Dunn, J.V. Small, and K. Rottner. 2008. Arp2/3 complex interactions and
843 actin network turnover in lamellipodia. *EMBO J.* 27:982-992. doi:
844 10.1038/emboj.2008.34.

845 Lauffenburger, D.A., and A.F. Horwitz. 1996. Cell migration: a physically integrated
846 molecular process. *Cell*. 84:359-369.

847 Lawson, C., S.T. Lim, S. Uryu, X.L. Chen, D.A. Calderwood, and D.D. Schlaepfer. 2012.
848 FAK promotes recruitment of talin to nascent adhesions to control cell motility. *J. Cell*
849 *Biol.* 196:223-232. doi: 10.1083/jcb.201108078.

850 Le Clainche, C., and M.F. Carlier. 2008. Regulation of actin assembly associated with
851 protrusion and adhesion in cell migration. *Physiol. Rev.* 88:489-513. doi:
852 10.1152/physrev.00021.2007.

853 Lingor, P., N. Teusch, K. Schwarz, R. Mueller, H. Mack, M. Bahr, and B.K. Mueller.
854 2007. Inhibition of Rho kinase (ROCK) increases neurite outgrowth on chondroitin
855 sulphate proteoglycan in vitro and axonal regeneration in the adult optic nerve in vivo. *J.*
856 *Neurochem.* 103:181-189. doi: 10.1111/j.1471-4159.2007.04756.x.

857 Liu, X., J. Huai, H. Endle, L. Schluter, W. Fan, Y. Li, S. Richers, H. Yurugi, K.
858 Rajalingam, H. Ji, H. Cheng, B. Rister, G. Horta, J. Baumgart, H. Berger, G. Laube, U.

859 Schmitt, M.J. Schmeisser, T.M. Boeckers, S. Tenzer, A. Vlachos, T. Deller, R. Nitsch,
860 and J. Vogt. 2016. PRG-1 Regulates Synaptic Plasticity via Intracellular PP2A/beta1-
861 Integrin Signaling. *Dev. Cell*. 38:275-290. doi: 10.1016/j.devcel.2016.06.019.

862 Lyons, D.M., P.S. Buckmaster, A.G. Lee, C. Wu, R. Mitra, L.M. Duffey, C.L.
863 Buckmaster, S. Her, P.D. Patel, and A.F. Schatzberg. 2010. Stress coping stimulates
864 hippocampal neurogenesis in adult monkeys. *Proc. Natl. Acad. Sci. U. S. A.* 107:14823-
865 14827. doi: 10.1073/pnas.0914568107.

866 Machesky, L.M., and A. Hall. 1997. Role of actin polymerization and adhesion to
867 extracellular matrix in Rac- and Rho-induced cytoskeletal reorganization. *J. Cell Biol.*
868 138:913-926. doi: 10.1083/jcb.138.4.913.

869 Machesky, L.M., and R.H. Insall. 1998. Scar1 and the related Wiskott-Aldrich syndrome
870 protein, WASP, regulate the actin cytoskeleton through the Arp2/3 complex. *Curr. Biol.*
871 8:1347-1356.

872 Matsui, T., M. Maeda, Y. Doi, S. Yonemura, M. Amano, K. Kaibuchi, S. Tsukita, and S.
873 Tsukita. 1998. Rho-kinase phosphorylates COOH-terminal threonines of
874 ezrin/radixin/moesin (ERM) proteins and regulates their head-to-tail association. *J. Cell*
875 *Biol.* 140:647-657.

876 McCarty, O.J., M.K. Larson, J.M. Auger, N. Kalia, B.T. Atkinson, A.C. Pearce, S. Ruf,
877 R.B. Henderson, V.L. Tybulewicz, L.M. Machesky, and S.P. Watson. 2005. Rac1 is
878 essential for platelet lamellipodia formation and aggregate stability under flow. *J. Biol.*
879 *Chem.* 280:39474-39484. doi: 10.1074/jbc.M504672200.

880 Michaelson, D., J. Silletti, G. Murphy, P. D'Eustachio, M. Rush, and M.R. Philips. 2001.
881 Differential localization of Rho GTPases in live cells: regulation by hypervariable regions
882 and RhoGDI binding. *J. Cell Biol.* 152:111-126. doi: 10.1083/jcb.152.1.111.

883 Mogilner, A., and G. Oster. 1996. Cell motility driven by actin polymerization. *Biophys. J.*
884 71:3030-3045. doi: 10.1016/S0006-3495(96)79496-1.

885 Monnier, P.P., A. Sierra, J.M. Schwab, S. Henke-Fahle, and B.K. Mueller. 2003. The
886 Rho/ROCK pathway mediates neurite growth-inhibitory activity associated with the
887 chondroitin sulfate proteoglycans of the CNS glial scar. *Mol. Cell. Neurosci.* 22:319-330.
888 doi: 10.1016/S1044-7431(02)00035-0.

889 Nobes, C.D., and A. Hall. 1995. Rho, rac, and cdc42 GTPases regulate the assembly of
890 multimolecular focal complexes associated with actin stress fibers, lamellipodia, and
891 filopodia. *Cell*. 81:53-62.

892 Ohtake, Y., D. Wong, P.M. Abdul-Muneer, M.E. Selzer, and S. Li. 2016. Two PTP
893 receptors mediate CSPG inhibition by convergent and divergent signaling pathways in
894 neurons. *Sci. Rep.* 6:37152. doi: 10.1038/srep37152.

895 Pasapera, A.M., I.C. Schneider, E. Rericha, D.D. Schlaepfer, and C.M. Waterman.
896 2010. Myosin II activity regulates vinculin recruitment to focal adhesions through FAK-
897 mediated paxillin phosphorylation. *J. Cell Biol.* 188:877-890. doi:
898 10.1083/jcb.200906012.

899 Pfurr, S., Y.H. Chu, C. Bohrer, F. Greulich, R. Beattie, K. Mammadzada, M. Hils, S.J.
900 Arnold, V. Taylor, K. Schachtrup, N.H. Uhlenhaut, and C. Schachtrup. 2017. The E2A
901 splice variant E47 regulates the differentiation of projection neurons via p57(KIP2)
902 during cortical development. *Development*. 144:3917-3931. doi: 10.1242/dev.145698.

903 Riddick, N., K. Ohtani, and H.K. Surks. 2008. Targeting by myosin phosphatase-RhoA
904 interacting protein mediates RhoA/ROCK regulation of myosin phosphatase. *J. Cell.*
905 *Biochem.* 103:1158-1170. doi: 10.1002/jcb.21488.

906 Ridley, A.J., M.A. Schwartz, K. Burridge, R.A. Firtel, M.H. Ginsberg, G. Borisy, J.T.
907 Parsons, and A.R. Horwitz. 2003. Cell migration: integrating signals from front to back.
908 *Science*. 302:1704-1709. doi: 10.1126/science.1092053.

909 Rottner, K., A. Hall, and J.V. Small. 1999. Interplay between Rac and Rho in the control
910 of substrate contact dynamics. *Curr. Biol.* 9:640-648.

911 Sabbatini, M.E., and J.A. Williams. 2013. Cholecystokinin-mediated RhoGDI
912 phosphorylation via PKCalpha promotes both RhoA and Rac1 signaling. *PLoS One*.
913 8:e66029. doi: 10.1371/journal.pone.0066029.

914 Savaskan, N.E., A.U. Brauer, and R. Nitsch. 2004. Molecular cloning and expression
915 regulation of PRG-3, a new member of the plasticity-related gene family. *Eur. J.*
916 *Neurosci.* 19:212-220. doi: 10.1046/j.1460-9568.2003.03078.x.

917 Sawada, K., K. Morishige, M. Tahara, Y. Ikebuchi, R. Kawagishi, K. Tasaka, and Y.
918 Murata. 2002. Lysophosphatidic acid induces focal adhesion assembly through

919 Rho/Rho-associated kinase pathway in human ovarian cancer cells. *Gynecol. Oncol.*
920 87:252-259. doi: 10.1006/gyno.2002.6831.

921 Sayas, C.L., A. Ariaens, B. Ponsioen, and W.H. Moolenaar. 2006. GSK-3 is activated by
922 the tyrosine kinase Pyk2 during LPA1-mediated neurite retraction. *Mol. Biol. Cell*.
923 17:1834-1844. doi: 10.1091/mbc.e05-07-0688.

924 Schaller, M.D., and J.T. Parsons. 1995. pp125FAK-dependent tyrosine phosphorylation
925 of paxillin creates a high-affinity binding site for Crk. *Mol. Cell. Biol.* 15:2635-2645.

926 Schmidt, S., and P. Friedl. 2010. Interstitial cell migration: integrin-dependent and
927 alternative adhesion mechanisms. *Cell Tissue Res.* 339:83-92. doi: 10.1007/s00441-
928 009-0892-9.

929 Schwab, M.E., J.P. Kapfhammer, and C.E. Bandtlow. 1993. Inhibitors of neurite growth.
930 *Annu Rev Neurosci*. 16:565-595. doi: 10.1146/annurev.ne.16.030193.003025.

931 Shaw, R.J., M. Henry, F. Solomon, and T. Jacks. 1998. RhoA-dependent
932 phosphorylation and relocalization of ERM proteins into apical membrane/actin
933 protrusions in fibroblasts. *Mol. Biol. Cell*. 9:403-419.

934 Sigal, Y.J., O.A. Quintero, R.E. Cheney, and A.J. Morris. 2007. Cdc42 and ARP2/3-
935 independent regulation of filopodia by an integral membrane lipid-phosphatase-related
936 protein. *J. Cell Sci.* 120:340-352. doi: 10.1242/jcs.03335.

937 Sinnett-Smith, J., J.A. Lunn, D. Leopoldt, and E. Rozengurt. 2001. Y-27632, an inhibitor
938 of Rho-associated kinases, prevents tyrosine phosphorylation of focal adhesion kinase
939 and paxillin induced by bombesin: dissociation from tyrosine phosphorylation of
940 p130(CAS). *Exp. Cell Res.* 266:292-302. doi: 10.1006/excr.2001.5219.

941 Somanath, P.R., and T.V. Byzova. 2009. 14-3-3beta-Rac1-p21 activated kinase
942 signaling regulates Akt1-mediated cytoskeletal organization, lamellipodia formation and
943 fibronectin matrix assembly. *J. Cell. Physiol.* 218:394-404. doi: 10.1002/jcp.21612.

944 Strauss, U., and A.U. Brauer. 2013. Current views on regulation and function of
945 plasticity-related genes (PRGs/LPPRs) in the brain. *Biochim. Biophys. Acta*. 1831:133-
946 138. doi: 10.1016/j.bbalip.2012.08.010.

947 Sutherland, C., J.A. MacDonald, and M.P. Walsh. 2016. Analysis of phosphorylation of
948 the myosin-targeting subunit of myosin light chain phosphatase by Phos-tag SDS-
949 PAGE. *Am. J. Physiol. Cell Physiol.* 310:C681-691. doi: 10.1152/ajpcell.00327.2015.

950 Takahashi, K., T. Sasaki, A. Mammoto, K. Takaishi, T. Kameyama, S. Tsukita, and Y.
951 Takai. 1997. Direct interaction of the Rho GDP dissociation inhibitor with
952 ezrin/radixin/moesin initiates the activation of the Rho small G protein. *J. Biol. Chem.*
953 272:23371-23375.

954 Tigyi, G., D.J. Fischer, A. Sebok, C. Yang, D.L. Dyer, and R. Miledi. 1996.
955 Lysophosphatidic acid-induced neurite retraction in PC12 cells: control by
956 phosphoinositide-Ca^{2+} signaling and Rho. *J. Neurochem.* 66:537-548.

957 Tkachenko, E., M. Sabouri-Ghomi, O. Pertz, C. Kim, E. Gutierrez, M. Machacek, A.
958 Groisman, G. Danuser, and M.H. Ginsberg. 2011. Protein kinase A governs a RhoA-
959 RhoGDI protrusion-retraction pacemaker in migrating cells. *Nat. Cell Biol.* 13:660-667.
960 doi: 10.1038/ncb2231.

961 Turner, C.E. 2000. Paxillin and focal adhesion signalling. *Nat. Cell Biol.* 2:E231-236.
962 doi: 10.1038/35046659.

963 van Helvert, S., C. Storm, and P. Friedl. 2018. Mechanoreciprocity in cell migration. *Nat.*
964 *Cell Biol.* 20:8-20. doi: 10.1038/s41556-017-0012-0.

965 Velmans, T., A. Battefeld, B. Geist, A.S. Farres, U. Strauss, and A.U. Brauer. 2013.
966 Plasticity-related gene 3 promotes neurite shaft protrusion. *BMC Neurosci.* 14:36. doi:
967 10.1186/1471-2202-14-36.

968 Webb, D.J., K. Donais, L.A. Whitmore, S.M. Thomas, C.E. Turner, J.T. Parsons, and
969 A.F. Horwitz. 2004. FAK-Src signalling through paxillin, ERK and MLCK regulates
970 adhesion disassembly. *Nat. Cell Biol.* 6:154-161. doi: 10.1038/ncb1094.

971 Webb, D.J., J.T. Parsons, and A.F. Horwitz. 2002. Adhesion assembly, disassembly
972 and turnover in migrating cells -- over and over and over again. *Nat. Cell Biol.* 4:E97-
973 100. doi: 10.1038/ncb0402-e97.

974 Wu, C., S.B. Asokan, M.E. Berginski, E.M. Haynes, N.E. Sharpless, J.D. Griffith, S.M.
975 Gomez, and J.E. Bear. 2012. Arp2/3 is critical for lamellipodia and response to
976 extracellular matrix cues but is dispensable for chemotaxis. *Cell*. 148:973-987. doi:
977 10.1016/j.cell.2011.12.034.

978 Yamashita, T., and M. Tohyama. 2003. The p75 receptor acts as a displacement factor
979 that releases Rho from Rho-GDI. *Nat. Neurosci.* 6:461-467. doi: 10.1038/nn1045.

980 Yoneda, A., H.A. Multhaupt, and J.R. Couchman. 2005. The Rho kinases I and II
981 regulate different aspects of myosin II activity. *J. Cell Biol.* 170:443-453. doi:
982 10.1083/jcb.200412043.

983 Yoshioka, K., S. Nakamori, and K. Itoh. 1999. Overexpression of small GTP-binding
984 protein RhoA promotes invasion of tumor cells. *Cancer Res.* 59:2004-2010.

985 Yu, P., C. Agbaegbu, D.A. Malide, X. Wu, Y. Katagiri, J.A. Hammer, and H.M. Geller.
986 2015. Cooperative interactions of LPPR family members in membrane localization and
987 alteration of cellular morphology. *J. Cell Sci.* 128:3210-3222. doi: 10.1242/jcs.169789.

988 Yu, P., T. Pisitkun, G. Wang, R. Wang, Y. Katagiri, M. Gucek, M.A. Knepper, and H.M.
989 Geller. 2013. Global analysis of neuronal phosphoproteome regulation by chondroitin
990 sulfate proteoglycans. *PLoS One*. 8:e59285. doi: 10.1371/journal.pone.0059285.

991 Zaidel-Bar, R., C. Ballestrem, Z. Kam, and B. Geiger. 2003. Early molecular events in
992 the assembly of matrix adhesions at the leading edge of migrating cells. *J. Cell Sci.*
993 116:4605-4613. doi: 10.1242/jcs.00792.

994 Zaidel-Bar, R., R. Milo, Z. Kam, and B. Geiger. 2007. A paxillin tyrosine phosphorylation
995 switch regulates the assembly and form of cell-matrix adhesions. *J. Cell Sci.* 120:137-
996 148. doi: 10.1242/jcs.03314.
997

Figure Legends

Figure 1. Cell migration is decreased in cells overexpressing PLPPR1. (A) Trajectories of Neuro2a cells transfected with EGFP (left) or EGFP-PLPPR1 (right), are plotted using the middle of each cell body as a point of reference. **(B)** Velocity and **(C)** total distance travelled of migrating cells were determined using NIS Elements software. Data represents mean ± SEM. EGFP, n = 38 cells; EGFP-PLPPR1, n = 52 cells. p-values were calculated using student's *t*-test with Welch's analysis, ****p<0.0001. Experiment was conducted in triplicate.

Figure 2. PLPPR1 increases cell adhesion. (A, B) Neuro2a cells expressing EGFP, EGFP-PLPPR1 or EGFP-PLPP1ΔC43 were detached with 5mM EDTA, replated on fibronectin coated 48-well plates and washed at 15, 30, 45 and 60min. Scale bar, 100μm. **(A)** Representative images at 15min before (top) and after washing (bottom). **(B)** Quantification of the percentage of adherent cells after washing at different time points. Data represents mean ± SEM. Individual p-values were calculated using Two-way ANOVA with Tukey's post-hoc analysis, ****p<0.0001. **(C)** Representative IRM images showing attachment of Neuro2a cells transfected with either EGFP (top) or EGFP-PLPPR1 (below) to the fibronectin substrate. Scale bar, 50μm. Inset is a higher magnification image of the boxed area. **(D)** Relative attachment of the cell to the fibronectin substrate was calculated by thresholding darker pixels divided by the traced cell area. A color map 'Gem' is used to display higher intensity pixels as blue and lower intensity as orange which represent stronger and weaker adhesions respectively. EGFP, n = 14 cells; EGFP-PLPPR1, n = 13 cells. Data represents mean ± SEM. p-

values were calculated using students *t*-test with Welch's analysis. **p<0.01. **(E)** Representative confocal images of cells overexpressing EGFP-PLPPR-1 cells (right) demonstrate trailing fibers (white arrow) which are absent in EGFP-transfected cells (left). Nuclei are stained with DAPI (blue). Scale bar, 50μm. **(F)** Representative IRM images of cells transfected with either EGFP (left) or EGFP-PLPPR1 (right). Inset is a higher magnification of boxed area showing trailing fibers in cells overexpressing PLPPR1. Scale bar, 50μm. **(G)** Representative images of cells co-expressing F-tractin (mApple-FTR-940) with either EGFP (left) or EGFP-PLPPR1 (right) showing some membrane protrusions are devoid of actin filaments. Scale bar, 50μm. Inset is a higher magnification image of the boxed area. All experiments were conducted in triplicate.

Figure 3.

PLPPR1 expression induces changes in actin polymerization. (A) Actin stress fibers in Neuro2a cells expressing either EGFP (left) or EGFP-PLPPR1 (right). Inset is a higher magnification of boxed area. Scale bar, 50μm. **(B)** FRAP analysis of actin polymerization in Neuro2a cells co-transfected with F-tractin (mApple-FTR-940) and either EGFP (top) or EGFP-PLPPR1 (bottom). Top images demonstrate cell morphology; the boxed areas were subjected to FRAP and imaged at the indicated times post bleaching. Scale bar, 50μm. **(C)** Graph shows fluorescence recovery over time in EGFP-transfected cells (black solid line) and cells overexpressing PLPPR1 (red dotted line). **(D, E)** $t_{1/2}$ and mobile fraction were determined using Matlab. Data represent mean ± SEM. p-values were calculated using Student's *t*-test with Welch's analysis. *p<0.05.

Figure 4. Focal adhesion contacts are increased in cells overexpressing PLPPR1. **(A)** Representative TIRF images of Neuro2a cells transfected with either EGFP or EGFP-PLPPR1, plated on fibronectin coated MatTek dishes and immunostained for paxillin and phalloidin for F-actin. White asterisks show structural difference of stress fibers in the lamellipodia. White arrows indicate focal adhesion (FA) contacts. Scale bar, 10μm. **(B)** Mean size and **(C)** mean fluorescence intensity of paxillin were determined from FAs isolated with a segmentation algorithm in ImageJ. Data represents mean ± SEM. p-values were calculated using Student's *t*-test with Welch's analysis, *$p<0.05$, ****$p<0.0001$. **(D)** Western blot of transfected Neuro2a cells, probed for pY31, paxillin, pY576 and FAK. Membranes were stripped and reprobed for GFP and ß-actin for loading control. **(E, F)** Densitometric analysis of phosphorylated protein versus total protein for paxillin and FAK was performed using Image Studio Lite. Data represents mean ± SEM. p-values were calculated using Student's *t*-test with Welch's analysis, *$p<0.05$. All experiments were performed in triplicate.

Figure 5. PLPPR1 attenuates LPA and CSPG induced neurite retraction by reducing RhoA activation. (A) Representative images showing EGFP (left) or EGFP-PLPPR1 (right) transfected hippocampal neurons cultured on either PLL (top) or PLL and CSPGs (bottom). Scale bar, 50μm. **(B)** Neurite outgrowth analysis of total neurite length and **(C)** longest neurite were assessed at 2 DIV using NeuronJ. EGFP/PLL, n = 112; EGFP-PLPPR1/PLL, n = 115; EGFP/CSPGs, n = 113; EGFP-PLPPR1, n = 134 neurons. Data represent mean ± SEM. p-values were calculated using Two-way

ANOVA with Tukey's posthoc analysis, **p<0.01, ***p<0.001, ****p<0.0001. **(D)** Time lapse imaging of Neuro2a cells transfected with either EGFP (top) or EGFP-PLPPR1 (bottom) and exposed to LPA. Black arrows indicate retracting neurites. White asterisks indicate nonretracting neurites. **(E)** Cell response was calculated as the percentage of transfected cells that retracted their neurites. Data represent mean ± SEM. p-values were calculated using Two-way ANOVA with Tukey posthoc analysis. *p<0.05, ****p<0.0001. Scale bar, 50μm. **(F)** RhoA-GTP was pulled down using rhotekin-RBD beads from cell lysates prepared from transfected Neuro2a cells treated with either FAFBSA, 10% serum or 16μM LPA for 2min. I Immunoblots were probed for RhoA. ß-actin was used as loading control for total RhoA. Membranes were stripped and reprobed for GFP. **(G)** Densitometric analysis was performed using Image Studio Lite. Data represent mean ± SEM. p-values were calculated using Two-way ANOVA with Tukey posthoc analysis, *p<0.05, ***p<0.001. All experiments were conducted in triplicate.

Figure 6. PLPPR1 decreases LPA induced translocation and phosphorylation of MLC, MYPT1 and ERM proteins. (A) Representative images of serum starved Neuro2a cells expressing either EGFP or EGFP-PLPPR1 and exposed to FAFBSA or 16μM LPA for 2min were immunostained for pMLC. White arrows indicate localization of pMLC after LPA treatment in EGFP (top) and EGFP-PLPPR1 (bottom) transfected cells. White asterisks indicate the cell used for the profile plot in **B**. Scale bar, 50μm. **(B)** Profile plot showing distribution and localization of pMLC in transfected cells. **(C)** Differences in levels of pMLC was determined by assessing fluorescence intensity after

FAFBSA or LPA treatment using ImageJ. Immunoblots of cells transfected with either EGFP or EGFP-PLPPR1 and treated with FAFBSA, serum or LPA were probed for **(D)** GFP **(E)** pMLC and MLC **(G)** pMYPT1 and MYPT1 **(I)** pERM and ERM. **(F, H, J)** Densitometry analysis of phosphorylated protein versus total protein was performed using Image Studio Lite. Data represents mean ± SEM. p-values were calculated using Two-way ANOVA with Tukey posthoc analysis, *p<0.05, **p<0.01, ***p<0.001, ****p<0.0001 respectively. All experiments were performed in triplicate.

Figure 7. PLPPR1 maintains RhoA and Rac1 interaction with RhoGDI after LPA treatment. (A) Neuro2a cells expressing either EGFP, EGFP-PLPPR1 or EGFP-PLPPR1ΔC43 were subjected to immunoprecipitation with GFP-MA™ beads and immunoblotted with anti-RhoGDI antibody. Input was probed for GFP. **(B)** Serum starved transfected Neuro2a cells were treated with either FAFBSA, serum or LPA and subjected to immunoprecipitation with RhoGDI antibody. Immunoblots of input and immunoprecipitates were probed for either RhoGDI, RhoA or Rac1. Inputs were stripped and reprobed for GFP and ß-actin antibody for loading control. All experiments were conducted in triplicate.

Figure 8. Co-expression of constitutively active Rac1 with PLPPR1 rescues morphological change. (A) Representative confocal images of Neuro2a cells co-transfected HA-tag with either EGFP, EGFP-PLPPR1, EGFP-Rac1 T17N or cells co-expressing EGFP-PLPPR1 with EGFP-Rac1 G12V showing a rescue of the morphological change induced by overexpression of PLPPR1. Scale bar, 50μm. **(B)**

Rac1-GTP was pulled down using PAK-PBD beads from cell lysates prepared from Neuro2a cells co-transfected HA-tag with either EGFP, EGFP-PLPPR1, EGFP-Rac1 T17N or cells co-expressing with EGFP-PLPPR1 and EGFP-Rac1 G12V. Membranes were immunoblotted with Rac1 antibody. Membranes were stripped and reprobed with anti-GFP antibody. **(C)** Densitometric analysis of phosphorylated protein versus total protein was performed using Image Studio Lite. Data represents mean ± SEM. p-values were calculated using One-way ANOVA with Tukey posthoc analysis, **$p<0.01$, ****$p<0.0001$. **(D)** Cells transfected with either EGFP (top) or EGFP-PLPPR1 (bottom) were immunostained for Arp2/3, and phalloidin to visualize F-actin. White arrows indicate localization of Arp2/3. Inset is a higher magnification of boxed area. Scale bar, 50µm. All experiments were conducted in triplicate.

Figure 9. PLPPR1 modulates RhoA and Rac1 activity. Schematic showing the modulatory effect of PLPPR1 on RhoA and Rac1 activation through association with RhoGDI in response to CSPGs and LPA, to influence cell adhesion, cell migration and neurite outgrowth.

Movie S1. "Trailing fibers" observed in migrating PLPPR1 cells with Interference Reflection Microscopy.

Time lapse images of Neuro2a cells transfected with either EGFP or EGFP-PLPPR1 were acquired in bright field using Interference Reflection Microscopy (IRM) on Zeiss 780 LSM confocal microscope system using a 10×/0.45 NA objective lens. Movie shows 3min/frame.

Movie S2. Focal adhesions remain nascent in cells overexpressing PLPPR1 compared to EGFP-transfected cells.

Time lapse images of Neuro2a cells co-expressing mCherry-paxillin with either EGFP (left) or EGFP-PLPPR1 (right) were acquired on Delta Vision OMX microscope system using a 60×/1.49 NA TIRF objective lens. Movie highlight the size and nature of focal adhesions, including formation of trailing fibers in cells co-expressing mCherry-paxillin with EGFP-PLPPR1. Movie shows 3min/frame.

Movie S3. LPA induces neurite retraction and cell rounding in Neuro2a cells.

Serum starved Neuro2a cells were exposed to either FAFBSA (left) or 16μM LPA (right). Time lapse images were acquired on a Nikon A1R microscope with a 20×/0.75 dry objective lens with no time delay between frames for 20min. Movie shows 1min/frame.

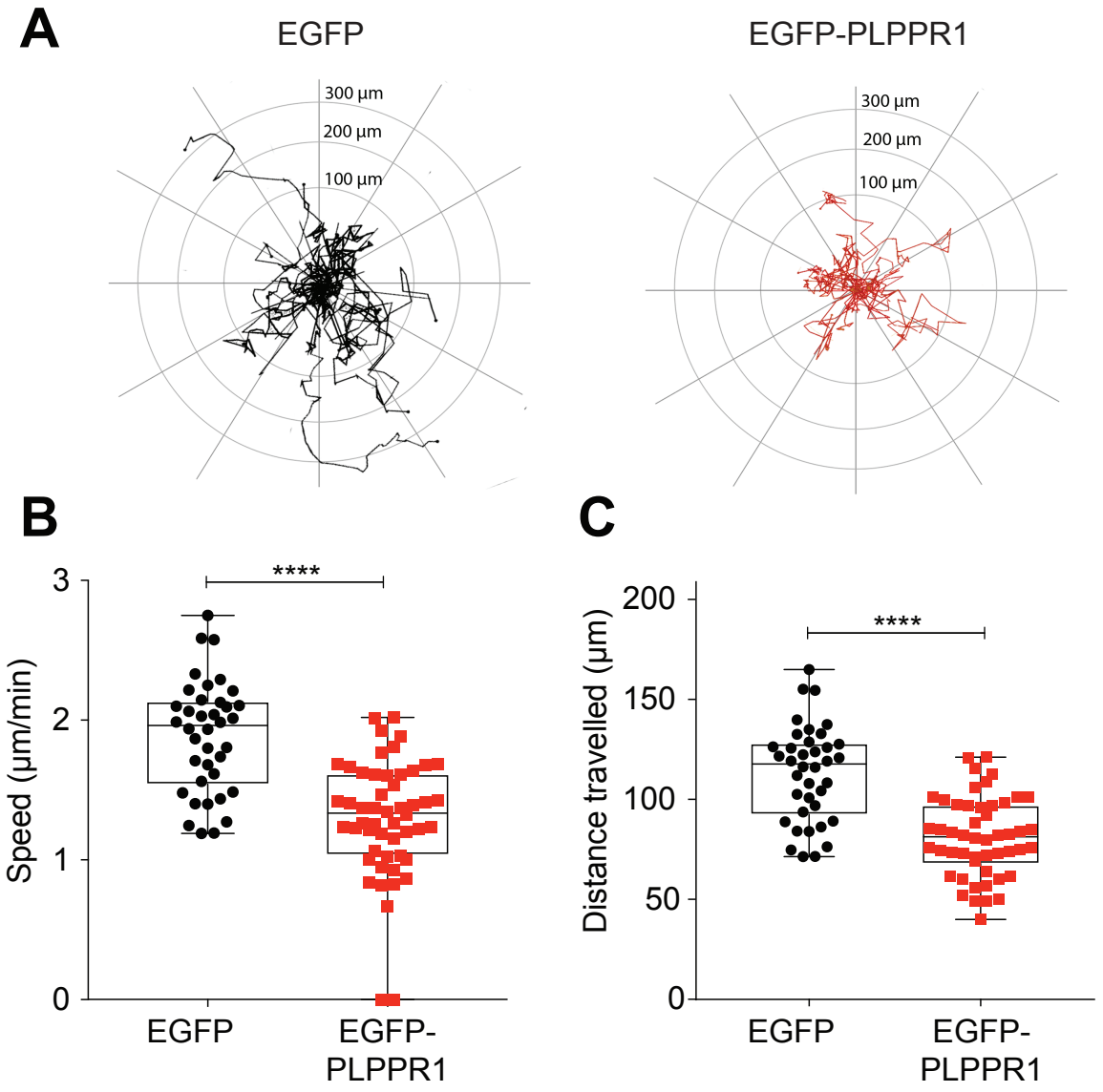
A
EGFP
EGFP-PLPPR1
300 µm
200 µm
100 µm
300 µm
200 µm
100 µm
B
C
****
Speed (µm/min)
3
2
1
0
EGFP
EGFP-PLPPR1
****
Distance travelled (µm)
200
150
100
50
0
EGFP
EGFP-PLPPR1

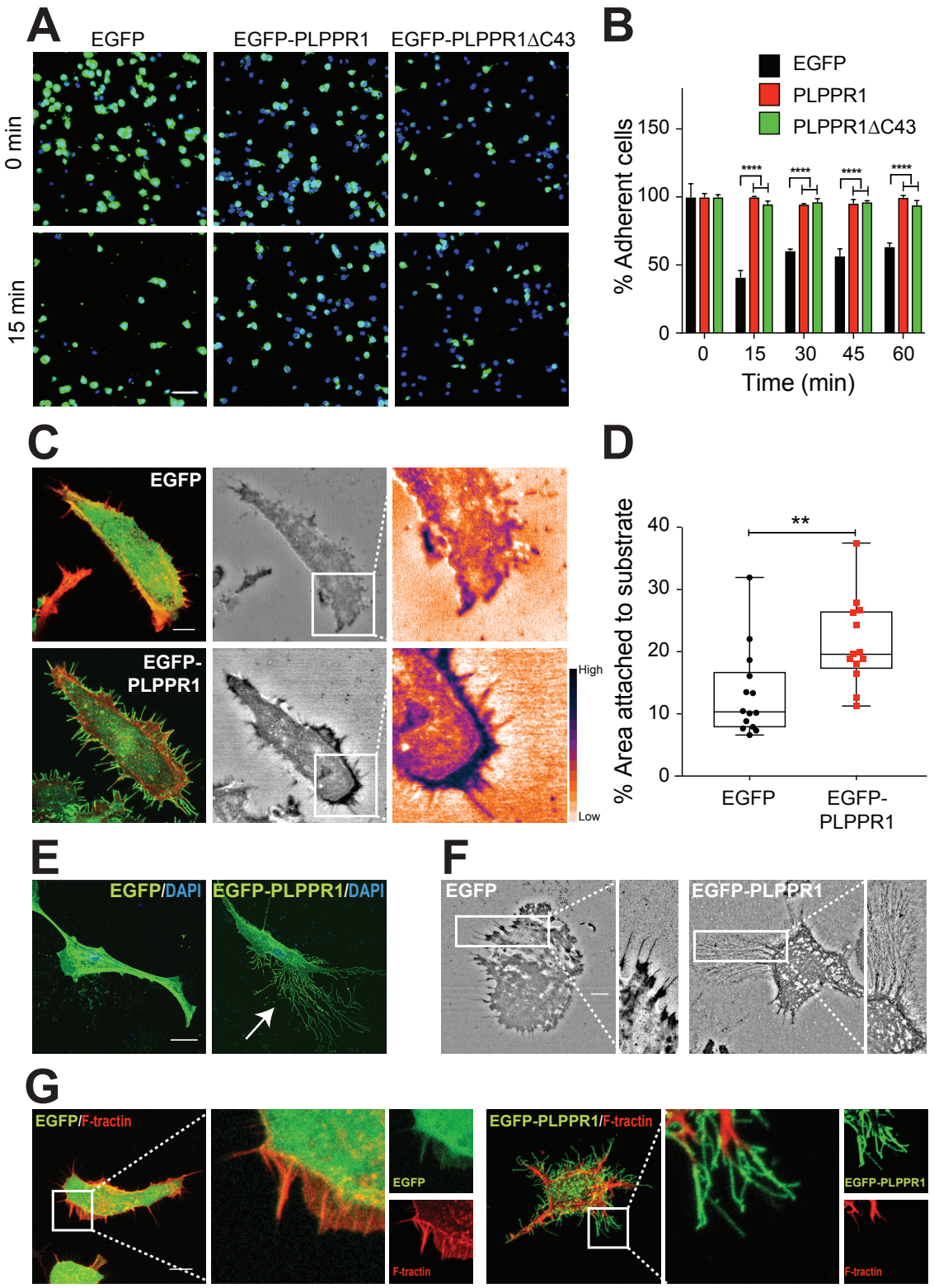
A
EGFP
EGFP-PLPPR1
EGFP-PLPPR1ΔC43
0 min
15 min
B
EGFP
PLPPR1
PLPPR1ΔC43
% Adherent cells
150
100
50
0
****
0
15
30
45
60
Time (min)
C
EGFP
EGFP-PLPPR1
High
Low
D
% Area attached to substrate
40
30
20
10
0
**
EGFP
EGFP-PLPPR1
E
EGFP/DAPI
EGFP-PLPPR1/DAPI
F
EGFP
EGFP-PLPPR1
G
EGFP/F-tractin
EGFP
F-tractin
EGFP-PLPPR1/F-tractin
EGFP-PLPPR1
F-tractin

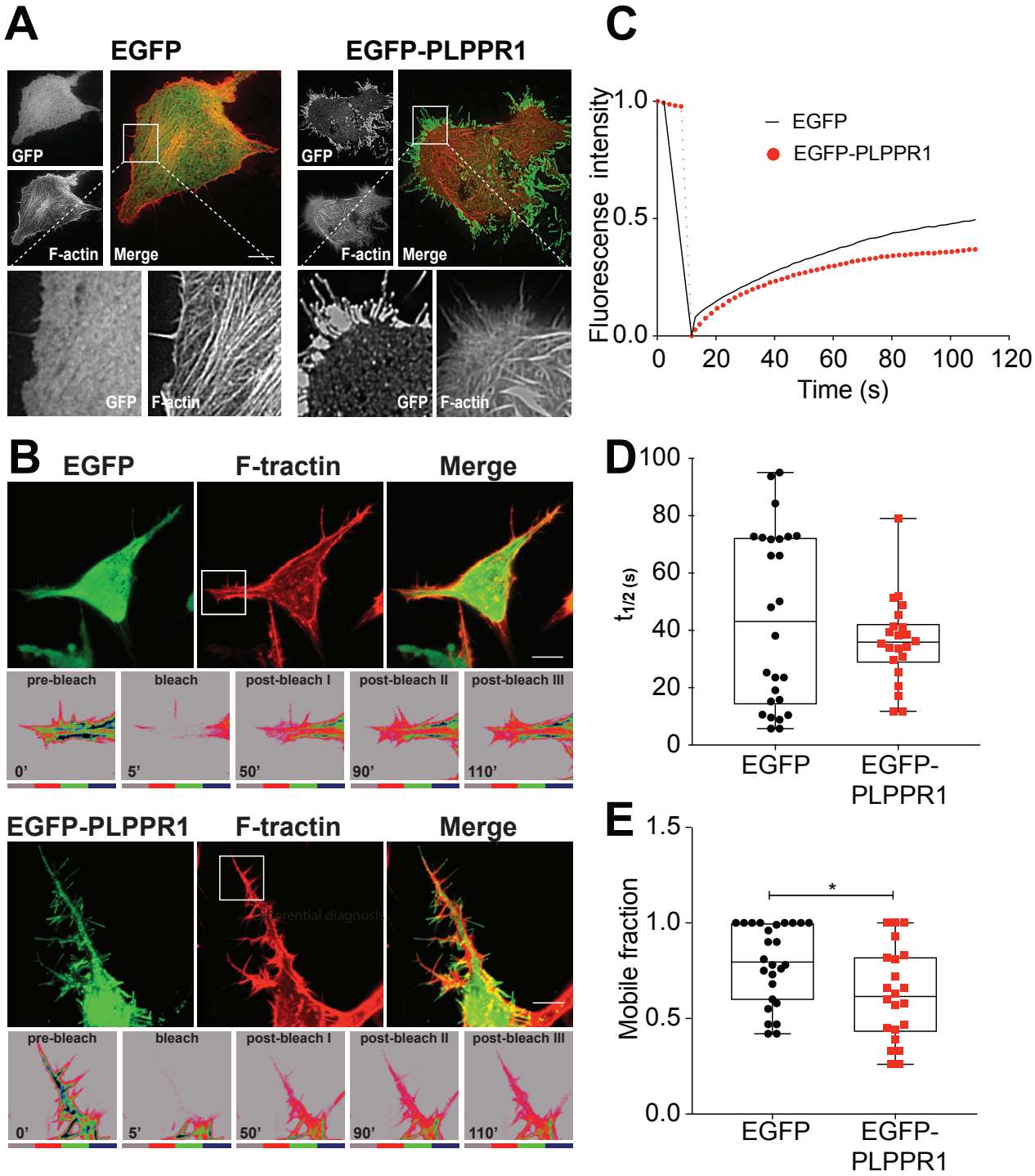
A
EGFP
EGFP-PLPPR1
GFP
F-actin
Merge
GFP
F-actin
Merge
GFP
F-actin
GFP
F-actin
B
EGFP
F-tractin
Merge
pre-bleach
bleach
post-bleach I
post-bleach II
post-bleach III
0'
5'
50'
90'
110'
EGFP-PLPPR1
F-tractin
Merge
pre-bleach
bleach
post-bleach I
post-bleach II
post-bleach III
0'
5'
50'
90'
110'
C
Fluorescense intensity
1.0
0.5
0.0
EGFP
EGFP-PLPPR1
0
20
40
60
80
100
120
Time (s)
D
$t_{1/2}$ (s)
100
80
60
40
20
0
EGFP
EGFP-PLPPR1
E
Mobile fraction
1.5
1.0
0.5
0.0
*
EGFP
EGFP-PLPPR1

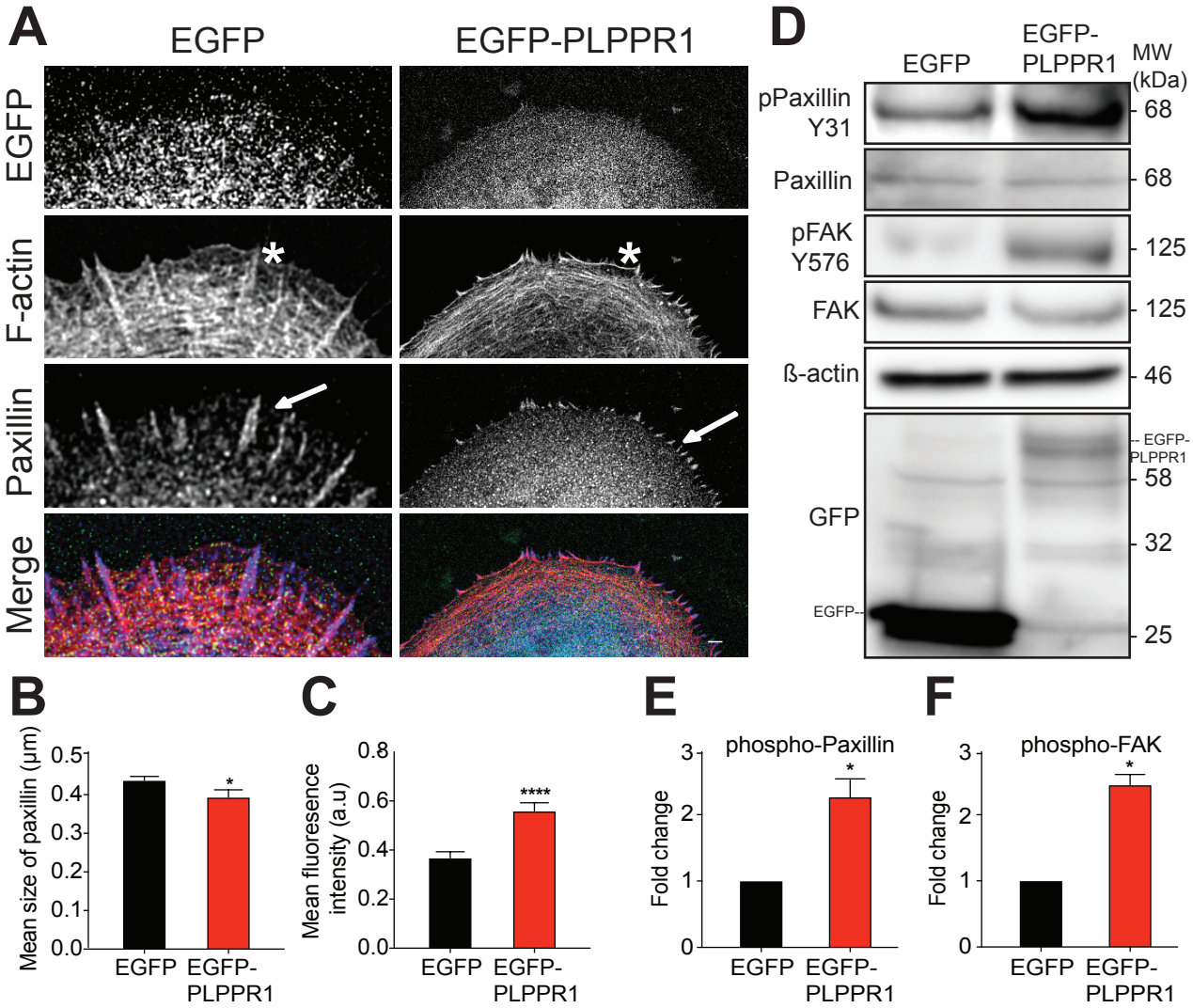
A
EGFP
EGFP-PLPPR1
EGFP
F-actin
Paxillin
Merge
D
EGFP
EGFP-PLPPR1
MW (kDa)
pPaxillin Y31
68
Paxillin
68
pFAK Y576
125
FAK
125
ß-actin
46
EGFP-PLPPR1
58
GFP
32
EGFP
25
B
Mean size of paxillin (µm)
0.5
0.4
0.3
0.2
0.1
0.0
*
EGFP
EGFP-PLPPR1
C
Mean fluoresence intensity (a.u)
0.8
0.6
0.4
0.2
0.0
****
EGFP
EGFP-PLPPR1
E
phospho-Paxillin
Fold change
3
2
1
0
*
EGFP
EGFP-PLPPR1
F
phospho-FAK
Fold change
3
2
1
0
*
EGFP
EGFP-PLPPR1

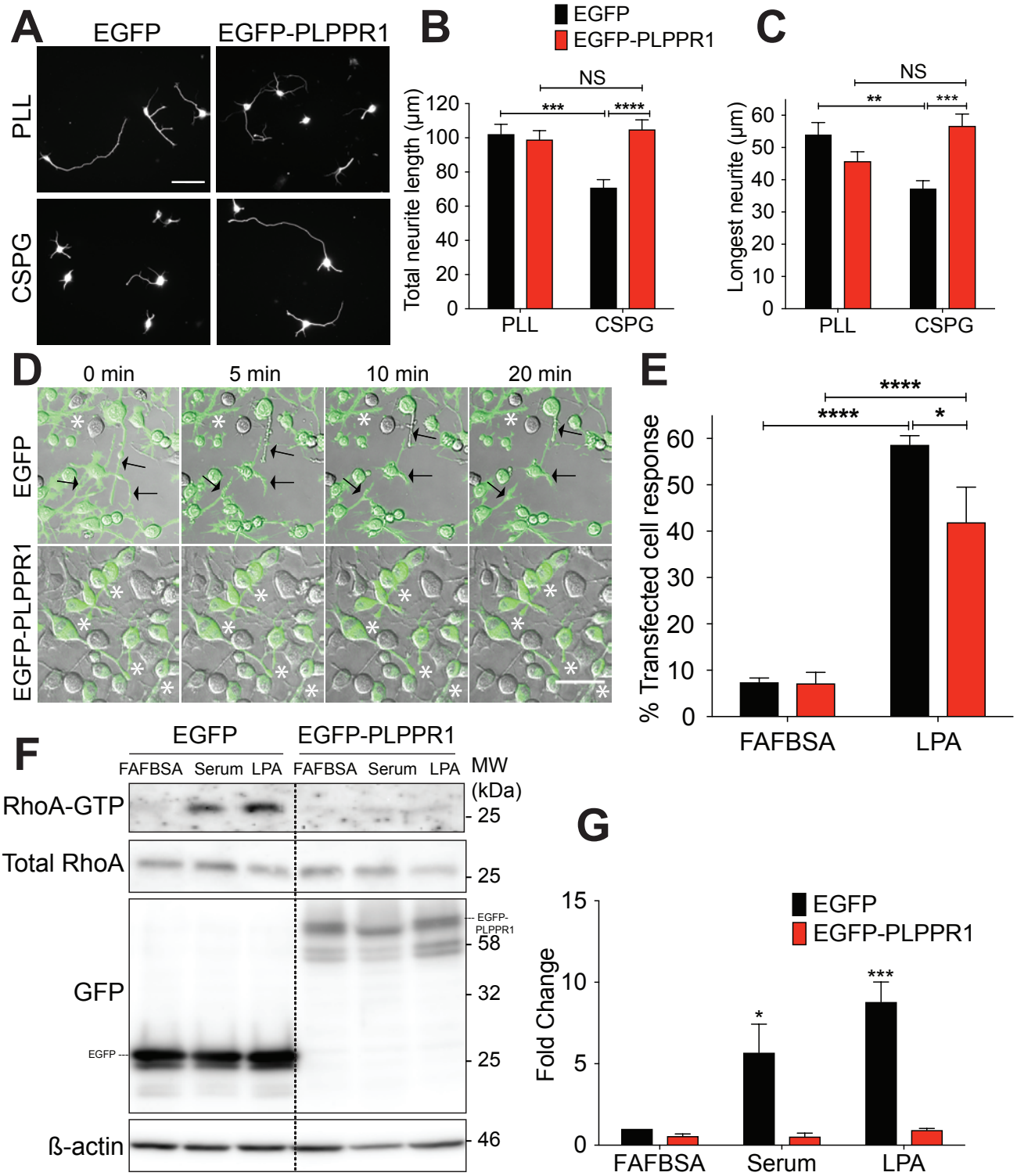
A
EGFP
EGFP-PLPPR1
PLL
CSPG
B
EGFP
EGFP-PLPPR1
NS
***
****
Total neurite length (µm)
120
100
80
60
40
20
0
PLL
CSPG
C
NS
**
***
Longest neurite (µm)
60
50
40
30
20
10
0
PLL
CSPG
D
0 min
5 min
10 min
20 min
EGFP
EGFP-PLPPR1
E
****
****
*
% Transfected cell response
60
50
40
30
20
10
0
FAFBSA
LPA
F
EGFP
EGFP-PLPPR1
FAFBSA
Serum
LPA
FAFBSA
Serum
LPA
MW
(kDa)
RhoA-GTP
25
Total RhoA
25
EGFP-
PLPPR1
58
GFP
32
EGFP
25
ß-actin
46
G
EGFP
EGFP-PLPPR1
Fold Change
15
10
5
0
*
***
FAFBSA
Serum
LPA

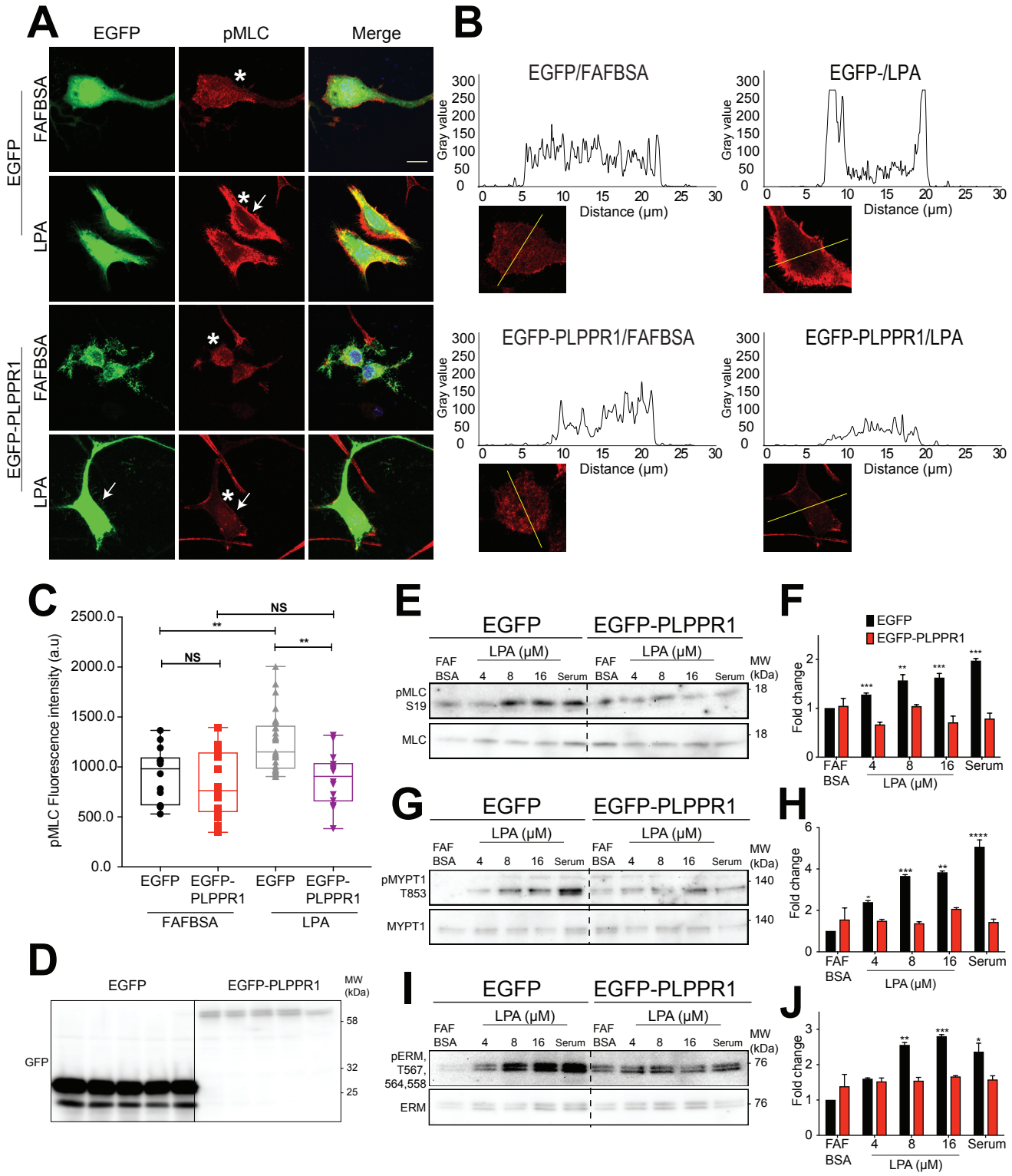
A
EGFP
pMLC
Merge
EGFP
FAFBSA
LPA
EGFP-PLPPR1
FAFBSA
LPA
B
EGFP/FAFBSA
EGFP-/LPA
EGFP-PLPPR1/FAFBSA
EGFP-PLPPR1/LPA
Gray value
Distance (μm)
C
pMLC Fluorescence intensity (a.u)
NS
**
EGFP
EGFP-PLPPR1
FAFBSA
LPA
D
EGFP
EGFP-PLPPR1
MW (kDa)
GFP
58
32
25
E
EGFP
EGFP-PLPPR1
LPA (μM)
FAF BSA
4
8
16
Serum
MW (kDa)
pMLC S19
MLC
18
F
EGFP
EGFP-PLPPR1
Fold change
G
pMYPT1 T853
MYPT1
140
H
I
pERM, T567, 564,558
ERM
76
J

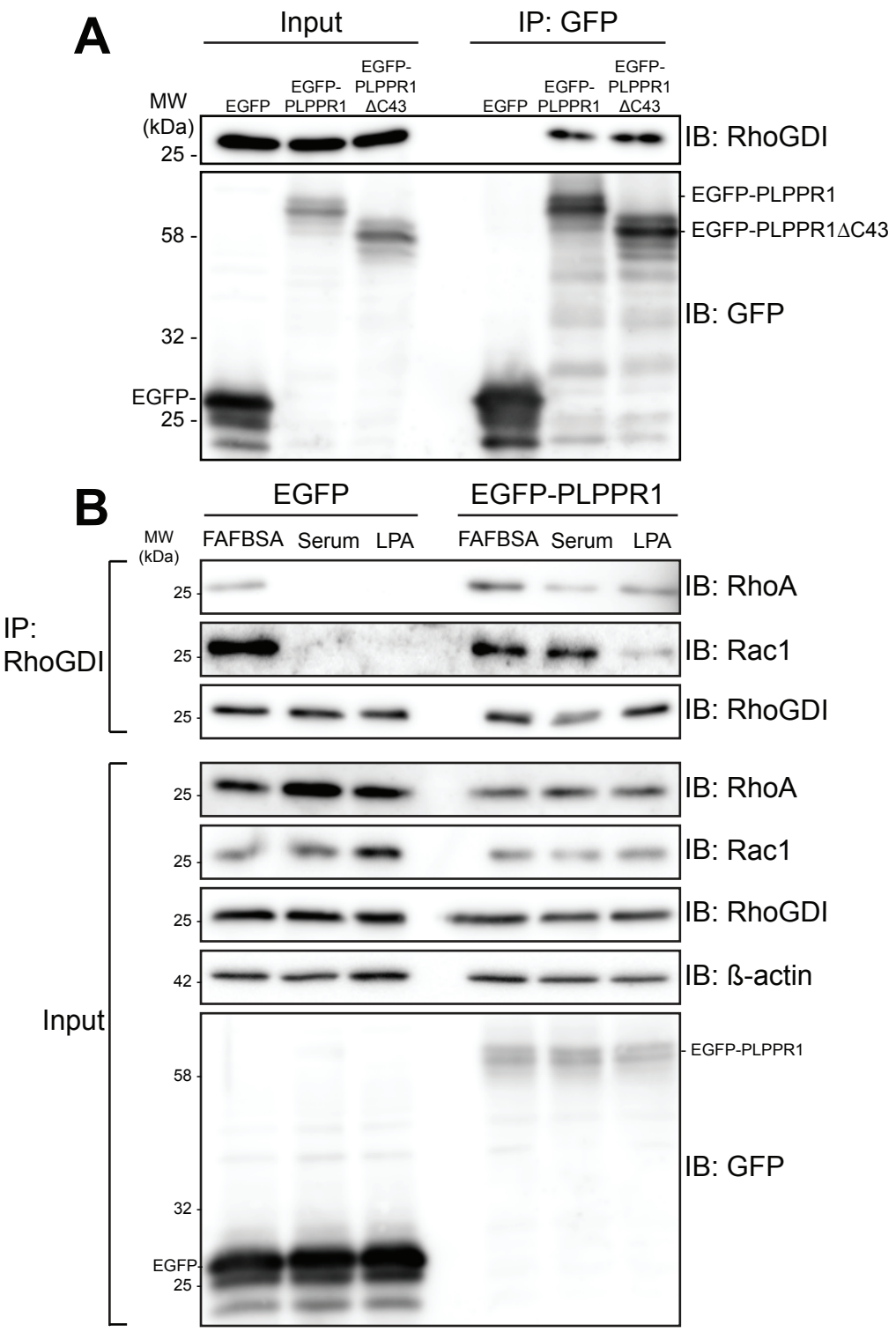
A
Input
IP: GFP
MW (kDa)
EGFP
EGFP-PLPPR1
EGFP-PLPPR1 ΔC43
EGFP
EGFP-PLPPR1
EGFP-PLPPR1 ΔC43
25
IB: RhoGDI
58
32
EGFP-
25
EGFP-PLPPR1
EGFP-PLPPR1ΔC43
IB: GFP
B
EGFP
EGFP-PLPPR1
MW (kDa)
FAFBSA
Serum
LPA
FAFBSA
Serum
LPA
IP: RhoGDI
25
IB: RhoA
25
IB: Rac1
25
IB: RhoGDI
Input
25
IB: RhoA
25
IB: Rac1
25
IB: RhoGDI
42
IB: ß-actin
58
EGFP-PLPPR1
IB: GFP
32
EGFP-
25

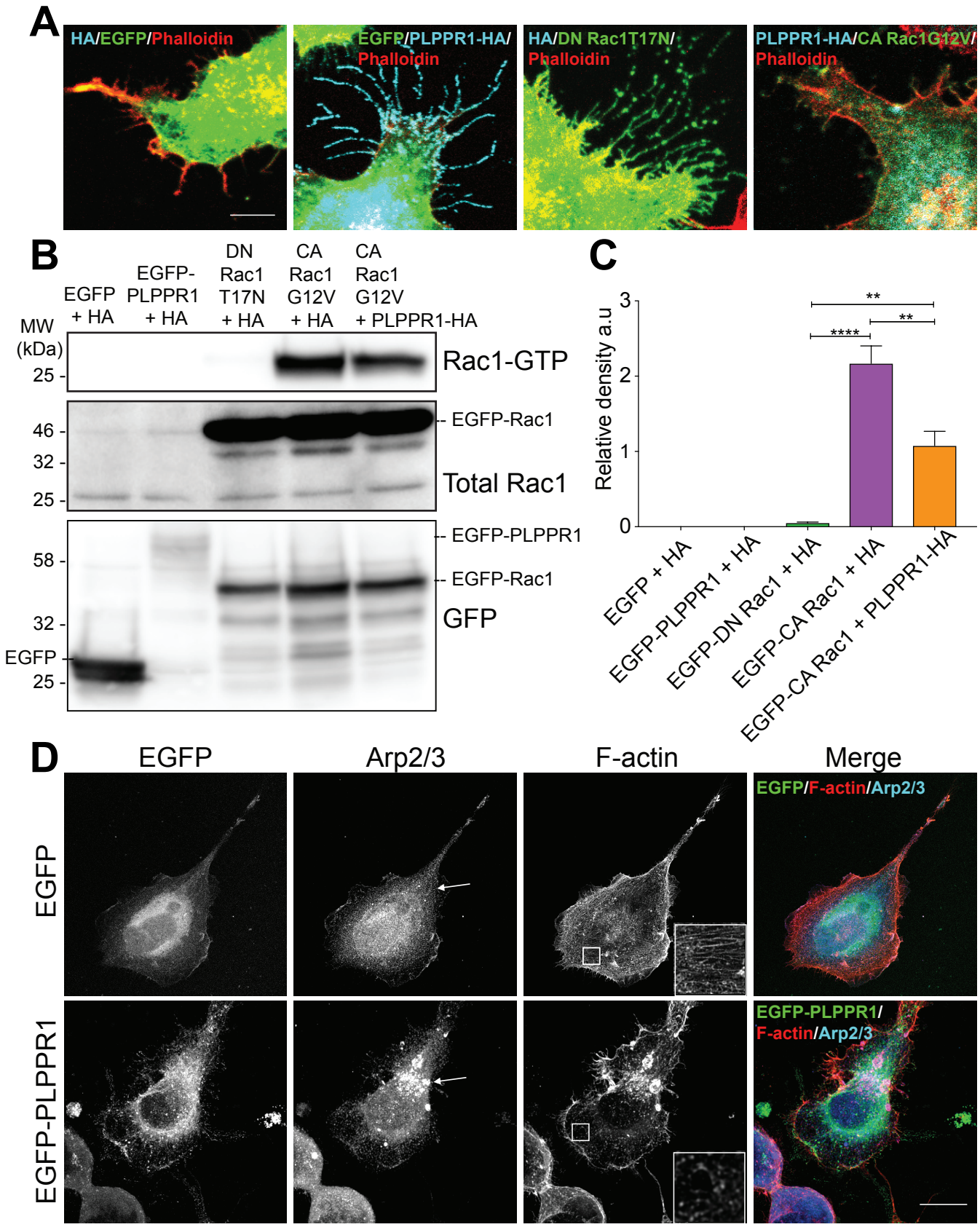
A
HA/EGFP/Phalloidin
EGFP/PLPPR1-HA/
Phalloidin
HA/DN Rac1T17N/
Phalloidin
PLPPR1-HA/CA Rac1G12V/
Phalloidin
B
EGFP
+ HA
EGFP-
PLPPR1
+ HA
DN
Rac1
T17N
+ HA
CA
Rac1
G12V
+ HA
CA
Rac1
G12V
+ PLPPR1-HA
MW
(kDa)
25
Rac1-GTP
46
32
25
EGFP-Rac1
Total Rac1
58
32
EGFP
25
EGFP-PLPPR1
EGFP-Rac1
GFP
C
Relative density a.u
3
2
1
0
**
**
****
EGFP + HA
EGFP-PLPPR1 + HA
EGFP-DN Rac1 + HA
EGFP-CA Rac1 + HA
EGFP-CA Rac1 + PLPPR1-HA
D
EGFP
Arp2/3
F-actin
Merge
EGFP
EGFP/F-actin/Arp2/3
EGFP-PLPPR1
EGFP-PLPPR1/
F-actin/Arp2/3

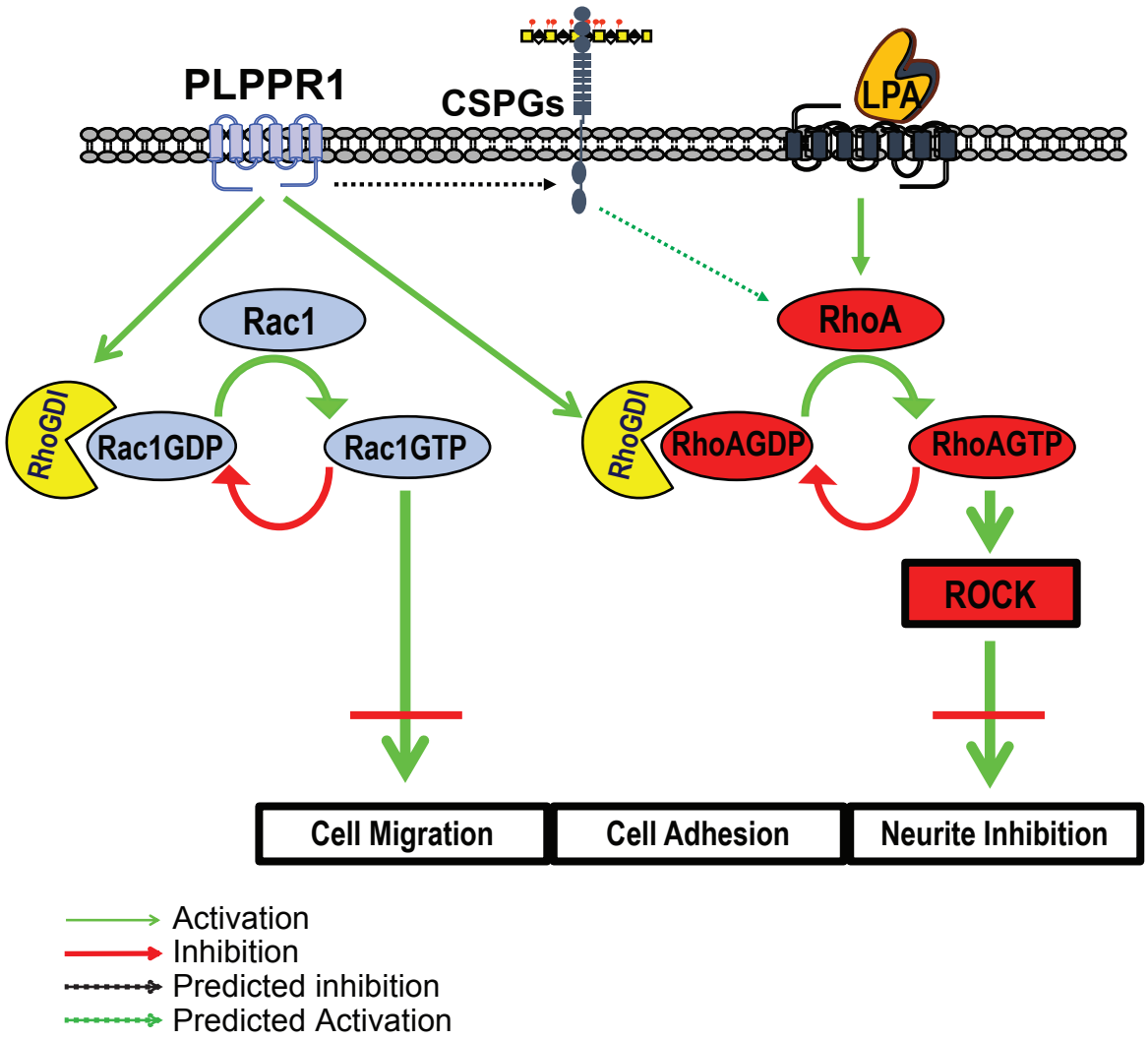
PLPPR1
CSPGs
LPA
Rac1
RhoGDI
Rac1GDP
Rac1GTP
RhoA
RhoGDI
RhoAGDP
RhoAGTP
ROCK
Cell Migration
Cell Adhesion
Neurite Inhibition
Activation
Inhibition
Predicted inhibition
Predicted Activation